Barium and Carbon fluxes in the Canadian Arctic Archipelago

Helmuth Thomas[1*], Elizabeth Shadwick[1,2], Frank Dehairs[3], Bruno Lansard[4], Alfonso Mucci[4], Jacques Navez[3], Yves Gratton[5], Friederike Prowe[6], Melissa Chierici[7], Agneta Fransson[8], Tim N. Papakyriakou[9], Erika Sternberg[1], Lisa A. Miller[10], Jean-Éric Tremblay[11], and Christophe Monnin[12]

[1]*Department of Oceanography, Dalhousie University, Halifax, NS, Canada*
[2]*now at: Antarctic Climate & Ecosystems Cooperative Research Center, Hobart, TAS, Australia*
[3]*Earth System Sciences & Analytical and Environmental Chemistry, Vrije Universiteit Brussel, Brussel, Belgium*
[4]*Department of Earth and Planetary Sciences, McGill University, Montreal, QC, Canada*
[5]*INRS-ETE, Québec, QC, Canada*
[6]*IFM-GEOMAR, Leibniz-Institut für Meereswissenschaften, D-24105 Kiel Germany*
[7]*Department of Chemistry, University of Gothenburg, Göteborg, Sweden*
[8]*Department of Earth Sciences, University of Gothenburg, Göteborg, Sweden*
[9]*Center for Earth Observation Science, University of Manitoba, Winnipeg, MB, Canada*
[10]*Institute of Ocean Sciences, Fisheries and Oceans, Canada, Sidney, BC, Canada*
[11]*Department de Biologie, Universite Laval, Quebec, Quebec, Canada*
[12]CNRS -Université Paul Sabatier, Laboratoire Mécanismes et Transferts en Géologie, Toulouse, France

**correspondence address: Email:* helmuth.thomas@dal.ca

Running head: Barium and Carbon in the Canadian Arctic

Abstract:

The seasonal and spatial variability of dissolved Barium (Ba) in the Amundsen Gulf, southeastern Beaufort Sea, was monitored over a full year from September 2007 to September 2008. Dissolved Ba displays a nutrient-type behavior: the maximum water column concentration is located below the surface layer. The highest Ba concentrations are typically observed at river mouths, the lowest concentrations are found in water masses of Atlantic origin. Barium concentrations decrease eastward through the Canadian Arctic Archipelago. Barite ($BaSO_4$) saturation is reached at the maximum dissolved Ba concentrations in the subsurface layer, whereas the rest of the water column is undersaturated. A three end-member mixing model comprising freshwater from sea-ice melt and rivers, as well as upper halocline water, is used to establish their relative contributions to the Ba concentrations in the upper water column of the Amundsen Gulf. Based on water column and riverine Ba contributions, we assess the depletion of dissolved Ba by formation and sinking of biologically bound Ba (bio-Ba), from which we derive an estimate of the carbon export production. In the upper 50 m of the water column of the Amundsen Gulf, riverine Ba accounts for up to 15% of the available dissolved Ba inventory, of which up to 20% is depleted by bio-Ba formation and export. Since riverine inputs and Ba export occur concurrently, the seasonal variability of dissolved Ba in the upper water column is moderate. Assuming a fixed organic carbon to bio-Ba flux ratio, carbon export out of the surface layer is estimated at 1.8±0.45 mol C m^{-2} yr^{-1}. Finally, we propose a climatological carbon budget for the Amundsen Gulf based on recent literature data and our findings, the latter bridging the surface and subsurface water carbon cycles.

1. INTRODUCTION

Barium (Ba) has increasingly been employed as water mass tracer and as biogeochemical proxy of biological productivity. Here, we combine both approaches in order to gain insights into the biogeochemistry of Ba and its relationship to the inorganic carbon cycle in the Canadian Arctic Archipelago. Finally, we use dissolved Ba data to assess export production of organic carbon, which in turn enables us to balance the carbon budget for our investigation area.

The strong correlation between the distributions of barium bound to particulate organic matter (bio-Ba) and particulate organic carbon (C_{org}) in the oceans and sediments has led to the use of bio-Ba as a proxy of biological productivity, in particular of export production from seasonal to geological time scales [e.g. *Bishop*, 1988; *Dehairs et al.,* 1992, 1997; *Dymond et al.*, 1992; *Francois et al.*, 1995; *Dymond and Collier*, 1996; *Gillikin et al.*, 2006; *Sternberg et al., 2007*; *Calvert and Peterson*, 2007]. As summarized by *Sternberg et al.* [2007], aggregates containing bio-Ba are formed in the upper water column. Accordingly, the highest bio-Ba concentrations are typically observed in surface waters, although such maxima may be less accentuated or missing in certain regions or seasons. A subsurface maximum of bio-Ba is also often observed in the mesopelagic layer and primarily consists of barite ($BaSO_4$) micro-crystals [*Bishop*, 1988; *Dehairs et al.*, 1997; *Jeandel et al.*, 2000; *Jacquet et al.*, 2007; *Sternberg et al.*, 2008; *Dehairs et al.*, 2008]. The presence of barite micro-crystals in oceanic suspended particulate matter is quite ubiquitous, despite the fact that most ocean waters are undersaturated with respect to this mineral [*Monnin et al.*, 1999]. Several hypotheses have been proposed to explain this conundrum [e.g. *Bishop*, 1988; *Dehairs et al.*, 1997; *Sternberg et al.*, 2005, 2008; *van Beek et al.*, 2009], most of which call upon biological processes including respiratory activity in the mesopelagic layer [*Dehairs et al.*, 1992]. A detailed review of these hypotheses can be found in *Sternberg et al*. [2007], and *Jacquet et al.* [2011] summarize these by reporting that barite precipitates in supersaturated microenvironments during the bacterial degradation of sinking organic

matter. In other words, organic particles that escape breakdown during settling through the water column, accumulate barite, thus explaining the observed depth-dependent increase of Ba fluxes [e.g. *Francois et al.*, 1995].

The continual formation of barite in biogenic aggregates, which settle through the water column, serves to increase Ba fluxes with depth and thus lowers the organic carbon to bio-Ba (C_{org}:bio-Ba) flux ratio with depth. Moreover, this ratio decreases with depth as a result of the (preferential) respiration of organic carbon relative to the release or dissolution of bio-Ba. Such observations have been reported in several, but not all regions of the deep oceans [*Dymond et al.*, 1992, *Francois et al.*, 1995], and thus the C_{org}:bio-Ba flux ratios recorded in ocean basins vary regionally [*Dymond et al.*, 1992; *Francois et al.*, 1995; *Dymond and Collier*, 1996]. On the other hand, *Dymond et al.* [1992] and *Francois et al*. [1995] have shown that within the euphotic zone and irrespective of the ocean basin, the C_{org}:bio-Ba flux ratio converges to a value of approximately C_{org}:bio-Ba=200 g C (g Ba)$^{-1}$ [2290 mol C (mol Ba)$^{-1}$], close to the globally estimated ratio C_{org}:bio-Ba=260 g C (g Ba)$^{-1}$ [2860 mol C (mol Ba)$^{-1}$] reported by *Broecker and Peng* [1982]. Higher C_{org}:bio-Ba flux ratios have been observed in continental margins [*Dehairs et al.*, 2000] and have been attributed to the formation of aggregates of both open ocean and margin carbon, and to differences in functioning of open ocean and marine ecosystems. Later in this paper, we exploit this fact to assess the export of marine carbon out of the euphotic zone, rather than an overall carbon export comprising terrestrial and marine carbon.

It is difficult to quantitatively relate the behaviour of particulate and dissolved Ba in the water column to each other, since, like Ca, dissolved Ba concentrations are 2-3 orders of magnitude larger than those of particulate Ba [e.g. *Jacquet et al.*, 2005, 2007]. Dissolved Ba displays a nutrient-type profile, which is, as we later argue, primarily shaped by the generation of bio-Ba in the surface layer and the subsequent release of Ba during the respiratory breakdown of the organic matter below the euphotic zone. In the mesopelagic and deep oceans, the formation and dissolution rates of barite

($BaSO_4$) also influence the vertical distributions and concentrations of dissolved Ba. Dissolved Ba has been employed as a water mass tracer in various ocean basins, including the Southern Ocean [e.g. *Jacquet et al.*, 2005, 2007; *Hoppema et al.*, 2010], and has been most useful in the Arctic Ocean, since Arctic rivers draining the North American continent carry significantly higher dissolved Ba concentrations than their Eurasian counterparts [e.g. *Cooper et al.*, 2008]. Few studies discuss factors that control the distribution of dissolved Ba in the water column of the Arctic region [e.g. *Falkner et al.,* 1994; *Guay and Falkner,* 1997; *Taylor et al.,* 2003; *Guay et al.,* 2009]. Complemented by additional tracers, such as total alkalinity (A_T) or the stable oxygen isotope composition of seawater ($\delta^{18}O$), dissolved Ba has been used to determine the nature/origin and contribution of freshwater (sea-ice melt and river runoff) to Arctic Ocean surface waters [e.g. *Falkner et al.*, 1994; *Guay and Falkner*, 1997, 1998; *Cooper et al.*, 2008; *Bates et al.*, 2009; *Yamamoto-Kawai et al.*, 2010]. In the surface waters, the concentrations of dissolved Ba reveal a high spatial variability with significantly enhanced concentrations of dissolved Ba close to the river mouths [e.g. *Guay et al.*, 2009; *Yamamoto-Kawai et al.*, 2010]. Likewise, the strong seasonality of river runoff is reflected in the temporal variability of the surface dissolved Ba concentrations in nearshore regions, a feature that has not been readily captured in recent studies because of the paucity of data during ice-covered seasons. In an attempt to circumvent this shortcoming, *Cooper et al.* [2008] introduced the use of flow-weighted values of tracer concentrations, such as Ba in Arctic rivers.

In the present work, we move beyond previous studies by documenting the spatial and temporal variability of dissolved Ba in waters of the Canadian Arctic Archipelago over a complete annual cycle, as well as the relationship between Ba and measurable parameters of the inorganic carbon system, specifically the dissolved inorganic carbon (DIC) and A_T. We use results of a multi-tracer water mass analysis to assess the temporal evolution of freshwater addition and removal to/from the surface waters over the annual cycle, and compute the surface layer dissolved Ba deficiency - the difference between

observed and “ideal” or conservative Ba concentrations - as a measure of bio-Ba formation. From this deficiency, we estimate the annual export of organic carbon (C_{org}) out of the euphotic zone and discuss the role of export and decay of bio-Ba below the surface layer in relation to the saturation state of waters with respect to barite.

2. METHODS

2.1. Investigation Area

This study was conducted in the framework of the International Polar Year on board the Canadian icebreaker CCGS Amundsen between September 2007 and September 2008. Sampling in the Canadian Arctic Archipelago (CAA) took place at the beginning and end of the 12-month cruise at stations along an east-west section from Baffin Bay into the Eastern Beaufort Sea (Fig. 1). The Amundsen Gulf, in the eastern Beaufort Sea (Fig. 1), was sampled through a full annual cycle, for the very first time, at approximately bi-weekly intervals, at somewhat higher frequency during spring and summer than during winter, when, by design, the ship was frozen into free-drifting floes for varying periods of time. For the subsequent annual analysis, we constructed an annual cycle of observational data acquired in an area defined by the boundaries: 70°N-72°N, 121.8°W-126°W (Fig. 1). Obviously, any considerations of interannual variability would exceed the limitations of our data set.

2.2. Analytical Methods

As part of the overall sampling program in the Amundsen Gulf [e.g. *Shadwick et al.*, 2011b], we collected seawater samples using a rosette system equipped with 24 12-L Niskin bottles at approximately 70 stations (including repeats at different times of the year). Vertical profiles of dissolved Ba concentrations were constructed from 8-12 depths per cast. Unfiltered seawater was transferred directly from the spigot of the Niskin bottles into 30 mL plastic bottles, acidified with 15 μL

of concentrated Suprapur hydrochloric acid and analyzed in the home laboratory using Isotope Dilution Sector Field Inductively Coupled Plasma Mass Spectrometry (SF-ICP-MS, Element 2, Thermo Finnigan). Briefly, 1 g of seawater was spiked with 0.7 g of a ^{135}Ba-spike solution yielding a ^{138}Ba/^{135}Ba ratio between 0.7 and 1 to minimize error propagation. Subsequently the sample was diluted with Milli-Q grade water to a final weight of 30 g. Blanks consisted of acidified (with nitric acid) Milli-Q water. Quantities of sample, spike and dilution water were accurately assessed by weighing. Reproducibility of our method is ±1.5% (RSD) as tested on repeat preparations of reference solutions. Average Ba values obtained for reference waters SLRS-3 and an in-house standard (OMP, a Mediterranean Sea standard prepared by C. Jeandel) were 13.48 ± 0.21 μg l^{-1} (1σ) with a RSD of 1.55% and 10.49 ± 0.29 μg l^{-1} (1σ) with RSD of 2.75%, respectively, in good agreement with certified values (SLRS-3: 13.4 ± 0.6 μg l^{-1} and OMP: 10.4 ± 0.2 μg l^{-1}). Overall precision (including sampling precision) based on 6 dissolved Ba profiles sampled in a hydrographically stable environment is ± 0.3 μg l^{-1} (1σ) with a RSD of 5%. Please refer to Dehairs et al. [2008] and Jacquet [2007] for further details. The Ba sampling was paralleled by sampling for the stable isotope composition of seawater (δ^{18}O), of which samples were stored in 13 mL screw-cap plastic test tubes without headspace. The δ^{18}O samples were analyzed at the Geological Survey of Canada Delta-Laboratory in Quebec City. Water samples were acidified to pH ranging from 6 to 7 with orthophosphoric acid and transferred without headspace to 4-mL vials containing 100 mg of copper to scavenge sulfide species and a few grains of activated charcoal to scavenge organic volatiles. After resting in the refrigerator for 5 days, 600 μL of water were transferred to a 10-mL vial on a Gas Bench II and equilibrated at 25°C for 5-7 days with a 0.5% CO_2 in nitrogen gas mixture. The CO_2 gas was introduced and analyzed in a Delta Plus mass ratio spectrometer. The oxygen isotope ratio is expressed on the δ^{18}O notation, defined as the ^{18}O/^{16}O ratio of a sample relative to the Vienna Standard Mean Ocean Water (V-SMOW) according to:

$$\delta^{18}O = \left(\left({}^{18}O/{}^{16}O\right)_{sample} / \left(\delta^{18}O/\delta^{16}O\right)_{V\text{-}SMOW} - 1\right) \times 10^3 [‰] \quad (1)$$

The oxygen isotope composition of seawater was measured to a precision of ±0.05‰, based on the analysis of random duplicate samples. DIC and A_T were sampled according to standard protocols [*Dickson et al.*, 2007] at much higher spatial and temporal resolution, yielding more than 2000 measurements. All samples were analyzed on board by coulometric (DIC) and potentiometric (A_T) titration using a VINDTA 3C (Versatile Instrument for the Determination of Titration Alkalinity, by Marianda, Germany). Alternatively, A_T was also measured onboard using an automated Radiometer® (Titrilab 865) potentiometric titrator operated in continuous titrant addition mode. Routine calibrations and analyses of Certified Reference Materials (provided by A. G. Dickson, Scripps Institution of Oceanography) ensured that the uncertainty of the DIC and A_T measurements was less than 0.5%. Details of the sampling and analytical methods, as well as in-depth scientific evaluations of the DIC and A_T data, have been provided by *Shadwick et al.* [2011a, b] and *Mucci et al.* [2010].

2.3. Water Mass Decomposition

As outlined in the following section, one of the objectives of this study was to establish a surface layer budget of dissolved Ba. Deviations from a conservative behavior of dissolved Ba were estimated and attributed to the formation of bio-Ba. Together with literature values for the C_{org}:bio-Ba ratio in particulate organic matter, we estimate the export production out of the surface mixed layer (SML). The maximum surface mixed layer depth in the Amundsen Gulf is approximately 50 m, as determined from the position of the pycnocline (Fig. 2, see also *Chierici et al.* [2011], their Fig. 2c; or *Shadwick et al.* 2011b]). We furthermore assess the dissolved Ba surplus concentrations in waters between 50 m depth and the level corresponding to the practical salinity (S_P) = 33.1 isopleth, in order

to evaluate whether decay of bio-Ba occurs within this depth interval, just below the euphotic zone.

In order to establish a dissolved Ba budget, we performed a regional water mass analysis in the upper water column, with the Upper Halocline Layer (UHL), characterized by $S_P = 33.1$ (Fig. 2), as the deepest layer. In the Amundsen Gulf, the UHL water resides at a depth of 80-120 m (Fig. 2). Our analysis thus encompasses the depth range of interest (0-50 m), as well as the layer between 50 m and $S_P = 33.1$ isopleth, located at approximately 100 m water depth for most of the year.

The application of salinity (S) and A_T to distinguish the two major sources of freshwater, river runoff and sea-ice melt, to seawater is well established [e.g., *Yamamoto-Kawai and Tanaka*, 2005]. Here, we employ a three end-member mixing model to decompose the water masses of the surface layer in fractions of upper halocline water (F_{UHL}), meteoric water (F_{MW}; river runoff + precipitation), and sea-ice melt (F_{SIM}). If the chemical properties of each end-member are distinct and well defined, the relative contributions of these three water masses to a parcel of seawater can be computed from the following equations:

$$F_{MW} + F_{SIM} + F_{UHL} = 1 \quad (2)$$

$$F_{MW}S_{MW} + F_{SIM}S_{SIM} + F_{UHL}S_{UHL} = S \quad (3)$$

$$F_{MW}A_{T(MW)} + F_{SIM}A_{T(SIM)} + F_{UHL}A_{T(UHL)} = A_T \quad (4.a)$$

$$F_{MW}\delta^{18}O_{(MW)} + F_{SIM}\,\delta^{18}O_{(SIM)} + F_{UHL}\,\delta^{18}O_{(UHL)} = \delta^{18}O \quad (4.b)$$

The decomposition was performed using two sets of equations: 2, 3 and 4a, as well as 2, 3 and 4b, meaning that we used either A_T or $\delta^{18}O$ together with salinity as tracers. In such analyses, as discussed for example by *Lansard et al.* [2011], each tracer has its individual strengths and weaknesses. For our purposes, relying on A_T tends to more accurately describe the contributions of sea-ice melt, at the expense of a slight underestimation of the river runoff. On the other hand, the use of $\delta^{18}O$, better

describes the river runoff fraction, but tends to underestimate the sea-ice fraction. Since we gathered much more high quality A_T data than $\delta^{18}O$ data, we used salinity together with A_T for the water mass decomposition analysis. Consequently, our estimate of riverine Ba input should be considered as a conservative, lower bound.

Table 1: End-members and characteristics used for the water mass decomposition analysis. All data were measured during our cruises. The meteoric water concentrations were measured in the Horton River Estuary during our program in spring 2008. $\delta^{18}O$ for sea-ice melt is adapted from *Bates et al.* [2009]. Salinity and A_T were used in the decomposition analysis, whereas Ba was used to compute the "ideal" Ba concentrations. Note that values quoted below may differ from those used in other studies [*Chierici et al.*, 2011, this issue] in the same area because of spatial and temporal variability. Furthermore, the null salinity and alkalinity ascribed to the sea-ice melt water reflect the integrated annual effect of the ice cycle.

	A_T [µmol kg^{-1}]	Salinity (S_P)	Ba [nM]	$\delta^{18}O$ [‰]
Meteoric water	1880.0	0	295	-20
Sea-ice melt	0	0	0	-2.0
Upper Halocline water	2283.0	33.1	69	-1.5

The end-member characteristics are given in Table 1. For the decomposition analysis, we assumed that S, A_T and the Ba concentration in sea-ice are null, i.e., on an annual cycle sea-ice does not constitute a net source or sink of these species to the underlying seawater. Rather these species are trapped during the ice formation in autumn and winter and are released again during ice melt. Considering the sea-ice concentrations of S, A_T, and Ba as being different from zero at annual or greater time scales, leads to an erroneous definition of ice as a source of these compounds, since the corresponding extraction during ice formation is ignored. If sea-ice concentrations are considered as different from zero, the water mass decomposition analysis will yield much larger meteoric fractions as a consequence [e.g. *Guay et al.*, 2009]. Furthermore, the effects of extraction and release of the above compounds on our analysis is so small as to be negligible for our purposes. The Ba concentrations in the Horton River Estuary are similar to those reported for other North American rivers [e.g. *Guay and Falkner*, 1998; *Cooper et al.*, 2008]. If we assume that there is only minor seasonal variability in the riverine Ba concentrations

[*Guay and Falkner*, 1998], the Horton River Ba concentration (295 nM Ba, Table 1) is close to the flow-weighted average concentrations of the nearby Mackenzie (371 nM Ba) or Yukon (369 nM Ba) Rivers [*Cooper et al*., 2008].

Using the fractions of the individual components F_{SW}, F_{SIM} and F_{UHL}, we computed the "ideal" Ba concentrations (Ba_{ideal}) in the upper water column down to S_P = 33.1, as outlined above.

$$F_{MW}Ba_{(MW)} + F_{SIM}Ba_{(SIM)} + F_{UHL}Ba_{(UHL)} = Ba_{ideal} \quad (5)$$

Ba_{ideal} represents the expected Ba concentration if Ba was a conservative property. For each sample, the difference between the actual, i.e., observed Ba concentration (Ba_{obs}), and Ba_{ideal} is used to compute the Ba deficiency, which we attributed to Ba export (Ba_{exp}) from the surface layer due to sinking of bio-Ba. In the discussion that follows we adopt a ratio of C_{org}:bio-Ba = 225 g C (g Ba)$^{-1}$ [2575 mol C (mol Ba)$^{-1}$], an approximate average of the values reported by *Dymond et al.* [1992], *Broecker and Peng* [1982] and *Francois et al.* [1995]. The *Broecker and Peng* [1982] estimate (C_{org}:bio-Ba=260 g C (g Ba)$^{-1}$) served as an upper bound, whereas values of C_{org}:bio-Ba=185-200 g C (g Ba)$^{-1}$, compiled by *Dymond et al.* [1992], are at the lower limit, with the value of C_{org}:bio-Ba=215 g C (g Ba)$^{-1}$, reported by *Francois et al.* [1995], ranging in between. The subsequent Ba inventory and carbon flux assessments were computed for the upper 50 m of the water column.

3. RESULTS AND DISCUSSION

3.1. Spatial Variability of Dissolved Ba Concentrations

Profiles from selected stations across the CAA show (Fig. 3) the lowest Ba concentrations (~40 nM) in the surface waters of eastern Baffin Bay and in the outflow of Lancaster Sound into Baffin Bay. The Ba profile recorded in the Amundsen Gulf (Fig. 3) displays a nutrient-type pattern with

surface water concentrations of approximately 50-60 nM Ba. The high Ba concentrations (65-70 nM Ba) in the subsurface waters of the CAA (Figs. 3, 4) correspond to an eastward flowing water mass [e.g. *Shadwick et al.*, 2011a] with a core salinity of 33.1, that is characteristic of the Pacific or Upper Halocline water mass. Irrespective of our sampling location, whether on the eastern or western side of the CAA, Ba concentrations converge to approximately 48 nM Ba in the deeper waters of Atlantic origin. In the western-most profile, at a near-shore station close to the Anderson River Estuary, Ba concentrations are elevated by runoff in the near surface layer but also display nutrient-like characteristics in the subsurface waters. In the surface waters of the eastern part of the CAA, the westward intrusion of water from Baffin Bay is evident from the low Ba concentrations (Fig. 4). It is also interesting to note the presence of the northward flowing West Greenland Current [e.g. *Münchow and Melling*, 2008], waters of Atlantic origin, characterized by low dissolved Ba concentrations, on the eastern side of Nares Strait (Fig. 4). The southward flowing waters on the western side of Nares Strait originate from the Arctic and are characterized by relatively high Ba concentrations, since the Arctic Ocean serves as collector for Arctic river water with elevated Ba concentrations [e.g. *Guay and Falkner*, 1998; *Cooper et al.*, 2008].

After the ice breakup in late April and early May, river runoff affects the surface waters, in particular in the western part of the study area (Fig. 5). The surface salinity minimum caused by both river runoff and sea-ice melt is usually observed in September, corresponding to the minimum sea-ice coverage [e.g., *Shadwick et al.*, 2011b]. In spring, i.e., during the months of May through July, we observed high dissolved Ba concentrations in nearshore areas, increasing in the westerly direction (Fig. 5a) caused by the arrival of riverine freshwater with high Ba concentrations. The early arrival of freshwater from rivers (compared to sea-ice melt) is also evident from the distribution of $\delta^{18}O$ in the mixed layer. Sea-ice $\delta^{18}O$-values are approximately -2‰ [*Bates et al.*, 2009], therefore the significantly more negative values recorded in the surface mixed layer in the western part of our study area (~-4‰)

reflect inputs from runoff with a $\delta^{18}O$ signature of approximately -20‰ [*Macdonald et al.*, 1989; *Cooper et al.*, 2008; *Bates et al.*, 2009; *Yi et al.*, 2009] (Fig 5b). As a consequence of the arrival of riverine freshwater, A_T decreases in the western areas (Fig. 5c), since riverine A_T concentrations are lower than A_T concentrations of the Amundsen Gulf [e.g., *Shadwick et al.*, 2011a]. At this time of the year (May-July), our observed $\delta^{18}O$ composition of the surface waters, which is in good agreement with the above mentioned literature values, reveals little or no contribution by fresh water from sea-ice melt, whereas the runoff fraction clearly increases in the westerly direction (Fig. 5d). The spatial distribution of the $\delta^{18}O$ composition in surface waters shows a clear east to west gradient (Fig. 5b) with values at -2‰ in the Amundsen Gulf indicating a low influence of river runoff here, and more negative values of -4‰ in the western part close to the estuaries. This agrees with findings by Magen et al. [2010], *Chierici et al.* [2011], and *Shadwick et al.* [2011a] that little or no runoff from the Mackenzie or Horton rivers reaches the Amundsen Gulf at any time of the year.

The relationship between dissolved Ba and DIC exposes two distinctly different regimes: the waters above and below the UHL (Fig. 6a, b). Within the Polar Mixed Layer (PML), a mixture of SIM, MW and UHL, covering approximately the upper 50 m of the water column and with a S_P range between 29.5 and 31, the concentrations of Ba and DIC are positively correlated and increase with depth until they reach values similar to those in the subsurface waters (50-100 m). Dissolved Ba concentrations are highest just above the UHL, originating from the Pacific at $S_P = 33.1$ (see also discussion in section 3.2.), while DIC continues to increase below the UHL due to the respiration of settling organic matter. Finally, both DIC and Ba concentrations decrease in deeper waters (Fig. 6a) as Atlantic Ocean Water is encountered. The A_T/Ba relationships (Fig. 6c, d) exhibit similar patterns to the DIC/Ba relationships, but given the more conservative behavior of A_T, relative to DIC, stronger linear correlations are observed in the sub-halocline waters. The addition of metabolic DIC occurs at timescales that are shorter or similar to the residence time of the subsurface waters in the Amundsen

Gulf (1-2 years [*Lanos*, 2009]; see also below section 3.4.), while the release of A_T and the dissolution or formation of barite occurs over longer, multi-year time scales, such that the A_T/Ba relationship appears to be dominated by water mass mixing (Fig. 6d).

We computed the Ba outflow from the Canadian Archipelago via Lancaster Sound in order to compare our observations with those of *Taylor et al.* [2003]. According to *Ingram* [2002, see also *Shadwick et al.*, 2011a] the outflow from Lancaster Sound into Baffin Bay is on the order of $1.1*10^6$ m^3 s^{-1}. Using this estimate, a depth-weighted water column average Ba concentration of 51.2 nM Ba (Fig. 3), and a water column depth of 500 m, yields an annual dissolved Ba export from the CAA into Baffin Bay on the order of $1.6*10^9$ mol Ba yr^{-1} or $222*10^9$ g Ba yr^{-1} (56.3 mol Ba s^{-1} / $7.7*10^3$ g Ba s^{-1}, respectively). *Taylor et al.* [2003] reported an outflow from the Canadian Archipelago of 89.7±7.6 mol Ba s^{-1}. Our estimate is smaller but of the same order of magnitude. *Taylor et al.* [2003] also considered the outflows from Jones Sound, Smith Sound, and Barrow Strait, whereas our estimate is restricted to the contribution from Lancaster Sound. Furthermore, it is worth noting that our depth-weighted average Ba concentration for Lancaster Sound (51.2 nM Ba) is slightly lower than the value reported by *Taylor et al.* [2003] (62.4±5.1 nM Ba).

3.2. Dissolved Ba and Barite Solubility in the Amundsen Gulf

We now investigate the temporal evolution of dissolved Ba concentrations and of the saturation state of the waters with respect to barite ($BaSO_4$) in the Amundsen Gulf (Figs. 7-9). The barite saturation state is expressed as:

$$Saturation\ state = \frac{Q_{(BaSO_4,aq)}}{K_{Sp(Barite)}} \quad (6)$$

where $Q_{(BaSO4,\,aq)}$ is the ion activity product of aqueous barium sulphate and $K_{sp\,(Barite)}$ is the thermodynamic solubility product of barite [*Monnin,* 1999]. The $BaSO_{4(aq)}$ ion activity product can be expressed as

$$Q_{(BaSO_4,aq)} = m_{Ba^{2+}(t,aq)} \cdot m_{SO_4^{2-}(t,aq)} \cdot \gamma^2_{BaSO_4(t,aq)} \qquad (7)$$

where *m* is the total molality of the designated aqueous species and γ is the total (or stoichiometric) mean activity coefficient of aqueous barium sulphate in seawater. The various thermodynamic quantities are calculated after *Monnin* [1999]. This model has been used to investigate the saturation state of the global ocean from the GEOSECS data [*Monnin et al.*, 1999]. A full description of the calculation of the barite saturation state from the measured quantities (dissolved Ba concentration, temperature, S_P and depth) is given by *Hoppema et al.* [2010].

As indicated in Fig. 3, dissolved Ba surface water concentrations are approximately 65.2±2.4 nM Ba in the upper 50 m of the Amundsen Gulf, and nearly invariant throughout the year, except for a slight decrease during the later part of the year (Fig. 7a). Within the subsurface layer, bounded by the SML and the S_P = 33.1 isopleth, the dissolved Ba concentrations reach maximum values of approximately 68.5±2.0 nM Ba. Here, as well, the concentrations appear to be relatively constant throughout the year (Fig. 7a). Below the UHL, the influence of deeper waters of Atlantic origin is reflected by decreasing Ba concentrations with depth to minimum values of approximately 45 nM Ba (Fig. 7a, 48.1±1.9 nM Ba below 200 m; 47.4±0.9 nM Ba below 300 m). The stable oxygen isotope composition of water (Fig. 7b) reveals lowest values of approximately $\delta^{18}O$ = -3.6‰ in the surface layer (-2.7±0.4‰ average in the upper 50m), and more positive values with depth to approximately $\delta^{18}O$ = -1.5‰ in the UHL layer at S_P = 33.1 (-1.7±0.4‰ average between 50m and

100m), and most positive values of $\delta^{18}O$ = 0.76‰ in the deep Atlantic layer (0.0±0.3‰ average below 200m, 0.0±0.3‰ average below 300m, 0.3±0.3‰ average below 500m).

In order to distinguish between the two major processes, that shape the nutrient-type barium profile: (1) the release of Ba from decaying organic matter in the layer just below the euphotic zone, and (2) the mixing of the surface and subsurface water masses, we consider the saturation state of the waters with respect to barite (Fig. 7c). The surface waters, i.e., the upper 50 m of the water column, are undersaturated with respect to barite throughout the year, particularly in June, which coincides with the maximum in net community production (NCP) [*Shadwick et al.*, 2011b, and discussion in section 3.3]; yet closer to saturation during ice-covered winter months than during the ice-free season. In the subsurface layer, between 50 m and 100 m depth, the saturation state values reach a maximum with barite saturation observed between June and February. This layer is undersaturated with respect to barite only during the winter months before the onset of NCP in the surface layer. To summarize, the highest barite saturation states are found between the S_P = 32 isopleth at approximately 50 m water depth and the S_P = 33.1 isopleth corresponding to the UHL (Fig. 7c), i.e., between the bottom of the surface mixed layer and the UHL. In the open ocean the bottom of the surface mixed layer typically corresponds to the depth of maximum respiration rates [e.g. *Aristegui et al.*, 2005]. The Amundsen Gulf is a shelf system and, clearly, is shallower than the open ocean, but nevertheless the maximum of respiratory activity, as indicated by the maximum of the ammonium concentrations (Fig. 9e), and the highest barite saturation states coincide with the bottom of the surface layer. The occurrence of a barite saturation state maximum is best visualized in property / property plots of selected hydrographic parameters and dissolved Ba concentrations or the barite saturation state (Fig. 8). The dissolved Ba versus salinity relationship highlights two distinct sections, each with nearly conservative behavior. A positive correlation of Ba and salinity is observed above the S_P = 33.1 horizon. While the S_P = 33.1 layer is characterized by an average Ba concentration of 69 nM Ba (Table 1), the maximum Ba

concentration is actually found at lower salinities, thus above the S_P = 33.1 isopleth. Below the S_P = 33.1 isopleth, dissolved Ba concentrations decrease with increasing salinity reaching a minimum in the deep waters of Atlantic origin (Fig. 8a). Similarly, the highest dissolved Ba values, and the only barite-equilibrated waters, are observed above the depths of the 33.1 isopleth (Fig. 8b) between approx. 50 m and 100 m depth (Fig. 7c). Above and below this level the water column is undersaturated with respect to barite. The group of particularly low barite saturation states at salinities of 30-31 is associated with warm waters in July (see for example *Shadwick et al.* [2011b], their Fig. 6b). Similar features arise when plotting dissolved Ba concentrations or the barite saturation state vs. $\delta^{18}O$: the $\delta^{18}O$ signature of the S_P = 33.1 isopleth is approximately $\delta^{18}O$ = -1.5‰ (Table 1), while both the dissolved Ba concentrations and the barite saturation state maximum correspond to values of $\delta^{18}O \approx$ -2‰ (Fig. 8c, d). Using the results of the subsequent water mass decomposition analysis down to the S_P level of 33.1 as a composite of MW, SIM, and UHL water (see eq. 2), we provide further evidence for the enrichment of dissolved Ba above the S_P = 33.1 layer. If we assume, as a thought experiment, that the meteoric Ba concentrations are zero (i.e., $Ba_{ideal}\{no\ Ba_{river}\}$) as detailed in the following section, the Ba versus salinity relationship becomes conservative and reflects a linear mixing of the PML and UHL waters (Fig. 8e, f). If we compare these results with our measurements, we see that in the salinity range between S_P = 32 and S_P = 33.1 the observed Ba concentrations and the barite saturation state appear elevated relative to the conservative Ba (i.e., $Ba_{ideal}\{no\ Ba_{river}\}$) versus S relationship. In fact, the only values corresponding to barite saturation correspond to those that deviate from the linear Ba vs. S relationship between the S_P = 32 and S_P = 33.1 (see empty circles and triangles in Fig. 8e, f). Since the contribution of MW to subsurface waters is negligible, we attribute the dissolved Ba surplus in the subsurface layer within the 32 to 33.1 S_P range to the release of Ba from decaying organic matter (bio-Ba_{decay}), which sank out of the surface layer (Fig. 9c, e). This Ba surplus peaks in late autumn, coinciding with the accumulation of dissolved organic carbon (DOC) and DIC in this subsurface layer

in response to organic matter decay (see *Shadwick et al.* [2011b], their Fig. 8c and d). Integrating this Ba surplus over the 50-100 m depth range yields a maximum Ba release of approximately 260 μM Ba m^{-2} (Fig. 9c), corresponding to approximately 40% of the bio-Ba formed in the surface layer (Fig. 10). The degradation of settling organic matter and the concomitant release of Ba to the water column explains the nutrient-like behavior of dissolved Ba. A further, biologically-mediated process affecting dissolved Ba concentrations is the precipitation of barite, which is associated with enhanced respiratory activity [e.g. *Dehairs et al.*, 1992]. This process, however, cannot be detected in our dissolved Ba measurements, since the amount of barite precipitation is approximately three orders of magnitude lower than the bio-Ba turnover.

3.3. Variability of Ba in the Amundsen Gulf and Export of Ba out of the Surface Layer

In order to arrive at an annual budget for dissolved Ba for the Amundsen Gulf area (Fig. 1), we employ a three end-member mixing model for the upper water column. The three end-members are meteoric water, sea-ice melt water and Upper Halocline Water, as defined by their respective A_T, salinity and $\delta^{18}O$ values (Table 1). The model yields the temporal evolution of their respective fractions over the course of the year. The maximum SIM contribution was 10% in October, whereas MW reached a maximum at 5% in the spring. Compared to the analysis of *Guay et al*. [2009], our values are higher for SIM and lower for MW, respectively. This discrepancy may reflect both a seasonal bias, as *Guay et al.* [2009] sampled only in summer during the salinity minimum, and the assumption that sea-ice constitutes a net annual source of salt. As noted previously this assumption is only valid at a seasonal time scale and at an appropriate spatial scale.

On the basis of the above mixing analysis, we computed "ideal" Ba concentrations (Ba_{ideal}) (Eq. 5) under the assumption that dissolved Ba behaves conservatively. In order to highlight the role of riverine dissolved Ba, we also show the observed Ba (Ba_{obs}), together with Ba_{ideal} and Ba_{ideal}{no

Ba_{river}}, the latter computed under the assumption that the MW does not carry any dissolved Ba (Figs. 8e, f). The Ba_{ideal}{no Ba_{river}} displays a near perfect conservative relationship to salinity, but it clearly underestimates Ba_{obs}. The riverine Ba contributed up to 15% of the Ba inventory in the upper 50 m of the water column (Fig. 10a). We attribute the deficiency between Ba_{obs} and Ba_{ideal} to Ba export (mainly as bio-Ba) out of the surface layer (Ba_{exp}, Fig. 8e) and computed Ba_{exp} for each observation throughout the annual cycle (Figs. 9, 10). The Ba deficiency in the surface layer and thus Ba_{exp} peaked in late summer/early autumn, when biological activity waned. The Ba_{exp} was lowest during the salinity maximum in late winter, just before the onset of increased biological activity triggered by longer daylight hours and ice melt, and shortly before the delivery of significant amounts of riverine Ba. In the subsurface layer below 50 m, Ba_{ideal} and Ba_{obs} are more similar (i.e., $Ba_{exp} = 0$), indicating that the bio-Ba is primarily formed in, and exported from, the euphotic zone. The onset of the Ba export out of the surface layer (Fig. 9c) is nicely mirrored by the rise of the ammonium (NH_4^+) concentrations [*Forest et al.*, 2011] in the subsurface layer (Fig. 9e), interpreted as an indicator of the arrival of sinking organic matter and is subsequent respiration. The high turnover rates of NH_4^+ prevent its accumulation in the water column, in contrast to the build-up of the Ba deficiency in the surface layer throughout the seasons. Within the subsurface layer, the build-up of the bio-Ba_{decay} (Fig. 9d) occurs somewhat delayed with respect to the onset of the Ba deficiency in the surface layer (Fig. 9c) and the beginning of enhanced NH_4^+ concentrations in the subsurface layer (Fig. 9e). On the other hand, as mentioned above, the rise of bio-Ba_{decay} appears concomitant to the increase of DOC concentrations in the subsurface layer [*Shadwick et al.*, 2011b, their Fig. 8d], as both originate from the decay of organic matter, and both are more stable than NH_4^+. The sinking rates of organic particles vary over a wide range, from a few meters to a few hundred meters per day [e.g. *Kellogg et al.*, 2011; *Armstrong et al.*, 2009]. Assuming slowly sinking particles with sinking rates <3 m d^{-1}, as reported for the investigation area [*Kellogg et al.*, 2011], the settling time would be on the order of 1-2 months. This would be in

general agreement with the findings discussed here, such as the delay between the rise of Ba_{exp} and bio-Ba_{decay} in the surface and subsurface layers, respectively (Fig. 9c, d).

3.4. Export Production of Carbon

We estimated the export of particulate organic carbon from the surface layer by assuming that it is tightly related to the bio-Ba flux [e.g. *Bishop*, 1988; *Dehairs et al.*, 1992, 1997; *Dymond et al.*, 1992; *Francois et al.*, 1995; *Dymond and Collier, 1996*; *Gillikin et al.*, 2006; *Sternberg et al.*, 2007; *Calvert and Peterson*, 2007] and that the latter can be computed from the dissolved Ba deficiencies in the upper 50 m of the water column (Fig. 8e). We employed an average ratio of C_{org}:bio-Ba= 225 g C (g Ba)$^{-1}$ [2575 mol C (mol Ba)$^{-1}$], adopted from *Dymond et al.* [1992], to estimate the export of particulate organic carbon from the surface layer. Our results indicate that the bio-Ba and organic carbon export fluxes from the upper 50 m of the water column (Fig. 10b) were smallest toward the end of winter (~0.3 mol C m^{-2}), before the onset of increased biological activity led by the proliferation of ice and under ice algae, when ice cover still persisted [e.g. *Horner and Schrader*, 1982; *Lavoie et al.*, 2009]. River runoff and the associated supply of riverine Ba lag behind the increase in Ba_{exp} (Fig. 10b), highlighting the contribution of ice algae and under-ice algae to the initial spring export of organic carbon out of the surface layer. The time lag between the onset of export production and the increased (under ice) carbon fixation, i.e., of net community production [NCP; see *Shadwick et al.*, 2011b], is consistent with the seasonal evolution of biological activity in the Canadian Arctic [*Horner and Schrader*, 1982; *Carmack et al.*, 2004; *Lavoie et al.*, 2009]. NCP remains high after the peak river discharge, but wanes in late summer, when heterotrophic processes begin to out-compete organic matter production. Around September, the export of organic matter, i.e., Ba_{exp}, reaches its maximum. From the perspective of the dissolved Ba pool, the riverine Ba was efficiently captured by bio-Ba formation, since the "new" Ba arrived just when biological activity was highest (Fig. 10b). This may

explain the lack of strong seasonality in dissolved (observed) Ba (Fig. 9b) profiles, as Ba_{exp} and $Ba_{riverine}$ displayed a similar seasonality (Figs. 10a, b; 9a, c), but with opposing effects on Ba_{obs}. Assuming that Ba_{exp} integrates the organic carbon export at the annual scale, the Ba_{exp} maximum corresponds to an annual organic carbon export of approximately 1.8 mol C m^{-2} yr^{-1}. Since estimates of primary productivity span over a rather wide range (4.4±1 mol C m^{-2} yr^{-1}, assuming that this result, obtained by *Forest et al.* [2011] for the period March-August, is representative for the entire year; 7-15 mol C m^{-2} yr^{-1}, based on satellite data [*Arrigo and van Dijken*, 2004]), and particle export studies cover only parts of the annual cycle [*Forest et al.*, 2011; *Magen et al.*, 2010], their relationship to our findings cannot readily be appreciated. Nevertheless, our estimated carbon export (1.8 mol C m^{-2} yr^{-1}) would represent 12-40% of the estimated primary production [*Arrigo and van Dijken*, 2004; *Forest et al.*, 2011], which is in a reasonable range [e.g., *Buesseler*, 1998]. It should be noted that the primary production estimate by *Arrigo and van Dijken* [2004] was derived from satellite observations and does not account for under-ice algal or subsurface production [e.g. *Tremblay et al.*, 2008; *Mundy et al.*, 2009]. *Shadwick et al.* [2011b] applied an inorganic carbon budget technique to derive a NCP of approximately 2.1 mol C m^{-2} yr^{-1} for the Amundsen Gulf region, 40% of which is supplied by under-ice productivity. According to our estimate, most of the NCP is exported out of the surface layer. Two independent, but similar estimates of the inventories of respired carbon dioxide (CO_2) in the subsurface waters (50-300 m) of the Amundsen Gulf were recently reported [*Shadwick et al.*, 2011b, a]: 3.8 mol C m^{-2} yr^{-1} and 4.1 mol C m^{-2}. The former was derived by assuming an 18-month residence time for subsurface waters [*Lanos*, 2009], in line with previous estimates [*Yamamoto-Kawai et al.*, 2008; *Hansell et al.*, 2004] in the region. Our estimate of export production (1.8 mol C m^{-2} yr^{-1}) and the respired CO_2 inventory of 4.1 mol C m^{-2} derived by *Shadwick et al.* [2011a] yield a residence time of the subsurface waters in the Amundsen Gulf on the order of two years, if all the exported carbon is respired in the subsurface waters, in agreement with the residence time reported by *Lanos* [2009].

The timing of the carbon export reconstructed from this study (Fig. 10b) is corroborated by *Forest et al.* [2008], who, based on sediment trap data, reported that the maximum POC contribution to the overall particle flux was observed in May and July, coinciding with the under-ice and pelagic algae blooms and their respective contributions to NCP [*Horner and Schrader*, 1982; *Shadwick et al.*, 2011b; see also *Carmack et al.*, 2004]. It should be noted, however, that the data of *Forest et al.* [2008] were collected in 2003/2004 and were acquired at a slightly different location. The latter may be of some importance since *Forest et al.* [2008] sampled west of our study area (Figs. 1, 5), likely under a stronger influence of the Mackenzie River plume. Our estimate of export production also depends on the choice of the C_{org}:bio-Ba flux ratio. The ratio we used in this study [C_{org}:bio-Ba= 225 g C (g Ba)$^{-1}$ or 2575 mol C (mol Ba)$^{-1}$] was derived from global or basin-wide estimates in various ocean basins. As noted by *Dymond et al.* [1992], their C_{org}:bio-Ba flux ratio (185-200 g C (g Ba)$^{-1}$) agrees to within 15% of the global estimate reported by *Broecker and Peng* [1982] (260 g C (g Ba)$^{-1}$). On the other hand, as argued by *Dehairs et al.* [2000] and *Sternberg et al.* [2007], the C_{org}:bio-Ba flux ratio may be higher along continental margins, but this has not yet been confirmed for the Arctic shelves. Irrespective of this, higher C_{org}:bio-Ba flux ratios have been attributed to higher carbon fluxes from coastal or margin sites, which in turn would allow our method to assess the export of marine carbon only. This would help constrain results of sediment trap studies, such as those of *Forest et al.* [2008, 2011] or *Magen et al*. [2010] by providing information about the source of the organic matter in the traps. A larger C_{org}:bio-Ba flux ratio would yield higher estimates of our carbon export and would exceed the NCP estimated by *Shadwick et al.* [2011b]. Furthermore, our estimate depends on the riverine Ba concentrations, such that an increase of the riverine Ba concentration by 33% (393 nM Ba instead of 295 nM Ba, Table 1) would increase the carbon export estimate by 24%. Despite the overall uncertainties of our approach, our estimated carbon export of 1.8 mol C m^{-2} yr^{-1}, derived from a complete annual data set, serves to better constrain carbon fluxes and production estimates. In addition,

since bio-Ba formation and, thus, the Ba fluxes out of the surface layer are closely linked to biological processes in the marine water column, our approach can help unravel the sources of settling organic particles, may they be marine or terrestrial, inorganic or organic [e.g. *Forest et al.*, 2008; *Magen et al.*, 2010].

3.5. The Role of Export Production in the Carbon Budget of Amundsen Gulf

In order to better understand the carbon dynamics of our study area, we establish a carbon budget over the annual cycle using our data and information available from the literature. We considered processes (Fig. 11) and assumptions detailed in this section. We derived the CO_2 air-sea exchange from *Shadwick et al.* [2011b], assuming that sea-ice is impermeable to CO_2, but acknowledge that the latter is currently a focus of ongoing research [e.g. *Semiletov et al.*, 2004; *Zemmelink et al.*, 2006; *Papakyriakou and Miller*, 2011; *Miller et al.*, 2011; *Else et al.*, 2011, this issue ; *Geilfus et al.*, 2011, this issue]. We considered the diffusion of DIC from the subsurface layer into the surface layer (upper 50 m) according to *Shadwick et al.* [2011b]. Since under-ice [*Horner and Schrader*, 1982; *Juul-Pedersen et al.*, 2010] and subsurface [*Tremblay et al.*, 2008] production plays a crucial role in Arctic Ocean productivity but cannot be captured by satellite imagery, we rely on the primary production estimate by *Forest et al.* [2011], employing a food web model for the period of our observations. We assume that this primary production estimate, obtained for the period March-August 2008, is representative of the overall annual production. We derived NCP from *Shadwick et al.* [2011b], who balanced the inorganic carbon budget in the water column of the Amundsen Gulf. Export production was assessed in this work and we assume that the export of particulate Ba mirrors the export of marine organic matter. Hence, given the export of marine carbon of 0.45 mol C m^{-2} yr^{-1} (see below) out of the subsurface layer (50-100 m), 1.35 mol C m^{-2} yr^{-1} of the 1.8 mol C m^{-2} yr^{-1} exported from the surface layer is respired in the subsurface layer. We considered two estimates for the respiration of organic

matter in the subsurface water column: (a) derived from an inorganic carbon budget [3.8 mol C m^{-2} yr^{-1}, *Shadwick et al.*, 2011b], and (b) using an estimate of the water column inventory of respired DIC according to *Shadwick et al.* [2011a]. The latter approach was applied to our investigation area, yielding an inventory of 4.1 mol C m^{-2}. Given an 18-month residence time for water below the surface layer, as estimated from a set of hydrographic moorings in the Amundsen Gulf in 2003-2004 [*Lanos*, 2009], this corresponds to an annual production of 2.7 mol C m^{-2} yr^{-1} for respiratory DIC. The particulate marine and terrestrial organic carbon flux out of the subsurface layer was estimated according to *Forest et al.* [2008, their Figure 8b]. This flux estimate, although from a slightly different area, covers almost a full year of observations, compared to that of *Forest et al.* [2011], which cover the period February to July. The extended temporal coverage by *Forest et al.* [2008] is of particular relevance, since our study, and *Forest et al.* [2008], reveal maximum C-export values during summer and autumn (Fig. 10), a period not covered by *Forest et al.* [2011]. The benthic respiration was estimated from the particle and sediment biogeochemical study of *Renaud et al.* [2007] using their average sediment oxygen demand of 5 mmol O_2 m^{-2} d^{-1}. When an O_2 consumption to metabolic CO_2 production ratio of 1.3 [*Millero*, 2006] is applied for either 6 or 12 months, benthic respiration yields a DIC release from the surface sediments to the overlying water column of 0.7-1.4 mol C m^{-2} yr^{-1}. We assume that there is no net sediment accumulation, i.e., no net carbon burial occurs over annual time-scales in the investigation area [*Richerol et al.*, 2008].

Despite the considerable uncertainties inherent to all estimated fluxes, the budget presented here can be considered as balanced. The ratio between primary production and NCP or export production [*Arrigo and van Dijken*, 2004; *Forest et al.*, 2011; *Shadwick et al.*, 2011b], respectively, all of which are derived from independent assessments, is on the order of 0.15-0.4. The similarity between the NCP and export fraction supports the hypothesis and observation that, at the annual scale, organic matter does not accumulate in the surface waters. The slightly elevated primary production to export

production ratio can be justified by the fact that the under-ice production, which contributes approximately 50% of NCP [*Shadwick et al.*, 2011b], is dominated by diatoms with heavy frustules that sink rapidly [*Horner and Schrader*, 1982; *Juul-Pedersen et al.*, 2010]. Furthermore, the spring open water bloom coincides with the peak in river runoff (Fig. 10b), which delivers a significant amount of ballast material from land and, in turn, promotes the sinking of marine organic matter, as observed in sediment trap studies [e.g. *Forest et al.*, 2008]. As a result of the respiration of pelagic and benthic, terrigenous and marine organic matter, the DIC in subsurface waters increases by 2.7-3.8 mol C m^{-2} yr^{-1} [*Renaud et al.*, 2007; *Richerol et al.*, 2008]. The magnitude of benthic respiration is similar to the export rate of terrigenous and marine organic matter from the subsurface layer. On the other hand, it should be stated that, given the uncertainties of the budget terms, including the residence time of the subsurface waters, we are presently unable to determine if lateral inputs of either organic matter or respired DIC to the study area are significant. It should also be noted that, since we compiled data from different years, our proposed budget reflects a climatological view rather than a budget for any specific year.

4. CONCLUSIONS

Dissolved Ba concentrations in the surface waters of the Canadian Arctic Archipelago display only a slight seasonality because the riverine inputs and the pulse in biological activity, which is accompanied by bio-Ba formation and export, occur nearly simultaneously. Formation and decay of bio-Ba shape the vertical nutrient-type profile of dissolved Ba in our study area, but the contribution of authigenic barite dissolution to the water column dissolved Ba concentrations cannot be distinguished. We exploited the seasonal Ba deficiency in the surface waters of the Amundsen Gulf to estimate the particulate organic carbon export out of the surface layer. This estimate, on the order of 1.8±0.45 mol C m^{-2} yr^{-1}, allowed us to construct a balanced carbon budget for the Amundsen Gulf.

Within this budget we identified and quantified relevant processes, including the export of particulate organic carbon and its subsequent respiration. Nevertheless, the role of lateral carbon transport into and out of our study area remains to be evaluated.

Acknowledgments. We express our sincere gratitude to the captains and crews who supported our work during the overwintering of the CCGS Amundsen. We are grateful to those who helped us sample for Barium and inorganic carbon parameters. This work is a contribution to the Canadian IPY programs CFL and GEOTRACES, Swedish Research Council, the Royal Society of Arts and Sciences, Swedish Research Council project #2004-4034, to ArcticNet, as well as to the IGBP/IHDP core project LOICZ. H. Thomas holds a Canada Research Chair. The manuscript greatly benefited from the comments of two anonymous referees.

References

Arístegui, J., S. Agustí, J.J. Middelburg, and C.M. Duarte, Respiration in the mesopelagic and bathypelagic zones of the oceans. In: P.A. del Giorgio and P.J.leB. Williams, Editors, *Respiration in Aquatic Ecosystems*, Oxford University Press, pp. 181–205, 2005.

Armstrong, R. A., M. L. Peterson, C. Lee, S. G. Wakeham, Settling velocity spectra and the ballast ratio hypothesis, *Deep Sea Research II*, 56(18), 1470-1478, 2009.

Arrigo, K. R., G. L. van Dijken, Annual cycles of sea ice and phytoplankton in Cape Bathurst polynya, southeastern Beaufort Sea, Canadian Arctic, *Geophys. Res. Lett.,* 31, L08304, doi:10.1029/ 2003GL018978, 2004.

Bates, N. R., J. T. Mathis, and L. W. Cooper, Ocean acidification and biologically induced seasonality of carbonate mineral saturation states in the Western Arctic Ocean, *J. Geophys. Res.,* 114, doi:10.1029/2008JC004862, 2009.

Bishop, J. B. K., The barite-opal-organic carbon association in oceanic particulate matter, *Nature,* 332, 341-344, 1988.

Broecker, W. S., and T.-H. Peng, Tracers in the Sea, Lamont-Doherty Geological Observatory, Palisades, New York, USA, 690pp, 1982.

Buesseler, K. O., The de-coupling of production and particulate export in the surface ocean, *Global Biogeochemical Cycles*, 12(2), 297–310, 1998

Calvert, S. E. and T. F. Pederson, Elemental Proxies for Palaeoclimatic and Palaeooceanographic Variability in Marine Sediments: Interpretation and Application. In: Proxies in the Late Cenozoic Paleoceanography, Hillaire-Marcel, C., and A. de Vernal (eds), Elsevier, Amsterdam, 567-644, 2007.

Carmack, E. C., R. W. Macdonald, and S. Jasper, Phytoplankton productivity on the Canadian Shelf of the Beaufort Sea, *Marine Ecology Progress Series,* 277, 37-50, 2004.

Chierici, M., A. Fransson, B. Lansard, L. A. Miller, A. Mucci, E. Shadwick, H. Thomas, J.-E. Tremblay, T. N. Papakyriakou, Magnitude and strength of biogeochemical processes and temperature on the Calcium Carbonate saturation in the Circumpolar Flaw Lead in the Amundsen Gulf, Arctic Ocean, submitted to *J. Geophys. Res.*, this special issue, 2011.

Cooper, L. W., J. W. McClelland, R. M. Holmes, P. A. Raymond, J. J. Gibson, C. K. Guay, and B. J. Peterson, Flow-weighted values of runoff tracers ($\delta^{18}O$, DOC, Ba, alkalinity) from the six largest Arctic rivers, *Geophys. Res. Lett.,* 35, L18606, doi:10.1029/2008GL035007, 2008.

Dehairs, F., W. Baeyens, and L. Goeyens, Accumulation of Suspended Barite at Mesopelagic Depths and Export Production in the Southern Ocean, *Science,* 258, 1332-1335, 1992.

Dehairs, F., D. Shopova, S. Ober, C. Veth, and L. Goeyens, Particulate barium stocks and oxygen consumption in the Southern Ocean mesopelagic water column during spring and early summer: relationship with export production, *Deep-Sea Res. II*, 44, 497-516, 1997.

Dehairs, F., N. Fagel, A. N. Antia, R. Peinert, M. Elskens, and L. Goeyens, Export production in the Bay of Biscay as estimated from barium-barite in settling material: a comparison with new production, *Deep-Sea Research I*, 47, 583-601, 2000.

Dehairs, F., S. Jacquet, N. Savoye, B. A. S. van Mooy, K.O. Buesseler, J. K. B. Bishop, C. H. Lamborg, M. Elskens M. Baeyens, P. W. Boyd, K. L. Casciotti, C. Monnin, Barium in twilight zone suspended matter as a potential proxy for particulate organic carbon remineralization: Results for the North Pacific. *Deep-Sea Res II*, 55, 1673-83, 2008.

Dickson, A. G., C. L. Sabine, and J. R. Christian, J.R. (Eds.), Guide to best practices for ocean CO_2 measurements, *PICES Special Publication*, 3, 191 pp, 2007.

Dymond, J., E. Suess, and M. Lyle, Barium in Deep-Sea Sediment: A Geochemical Proxy for Paleoproductivity, *Paleoceanography* **7**, 163-181, 1992.

Dymond, J. and R. Collier, Particulate barium fluxes and their relationships to biological productivity. *Deep-Sea Res. II* **43**, 1283-1308, 1996.

Else, B., T. Papakyriakou, R. Galley, W. Drennan, L. Miller, and H. Thomas, Eddy Covariance Measurements of Wintertime CO2 Fluxes in an Arctic Polynya: Evidence for Enhanced Air-Sea Gas Transfer During Ice Formation, *J. Geophys. Res.*, in press this issue, 2011.

Falkner, K. K., R. W. Macdonald, E. C. Carmack, and T. Weingartner, The Potential of Barium as Tracer of Arctic Water Masses, in The Polar Oceans and Their Role in Shaping the Global Environment, Johannessen, O. M., Muench, R.D., and Overland, J.E. (eds.), Geophysical Monograph 85, American Geophysical Union, 63-76, 1994.

Forest, A., M. Sampei, R. Makabe, H. Sasaki, D. G. Barber, Y. Gratton, P. Wassmann, and L. Fortier, The annual cycle of particulate organic carbon export in Franklin Bay (Canadian Arctic) Environmental Control and foodweb implications, *J. Geophys. Res.*, 113, C03S05, doi:10.1029/2007JC004262, 2008.

Forest, A., J.-É. Tremblay, Y. Gratton, J. Martin, J. Gagnon, G. Darnis, M. Sampei, L. Fortier, M. Ardyna, M. Gosselin, H. Hattor, D. Nguyen, R. Maranger, D. Vaqué, C. Marrasé, C. Pedrós-Alió, A. Sallon, C. Michel, C. Kellogg, J. Deming, E. H. Shadwick, H. Thomas, H. Link, P. Archambault, and P. Piepenburg, Biogenic carbon flows through the planktonic food web of the Amundsen Gulf (Arctic Ocean): A synthesis of field measurements and inverse modeling analyses, *Prog. Oceanography,* doi:10.1016/j.pocean.2011.05.002, in press, 2011.

Francois, R., S. Honjo, S. J. Manganini, and G. E. Ravizza, Biogenic barium fluxes to the deep sea: Implications for paleoproductivity reconstruction, *Global Biogeochem. Cycles*, 9, 289-303, 1995.

Geilfus, N.-X., G. Carnat, T. Papakyriakou, J.-L. Tison, B. Else, H. Thomas, E. Shadwick and B. Delille, pCO_2 dynamics and related air-ice CO_2 fluxes in the Arctic coastal zone (Amundsen Gulf, Beaufort Sea, Canada), subm. to *J. Geophys. Res.*, 2011.

Gillikin, D. P., F. Dehairs, A. Lorrain, D. Steenmans, W. Baeyens, and L. André, Barium uptake into shells of the common mussel (Mytilus edulis) and the potential for estuarine paleo-chemistry reconstruction, *Geochim. Cosmochim. Acta*, 70, 397-407, 2006.

Guay, C. K., and K. K. Falkner, Barium as tracer of Arctic halocline and river waters. *Deep-Sea Res. II*, 44, 1543-1569, 1997.

Guay, C. K., and K. K. Falkner, A survey of dissolved barium in the estuaries of the major Arctic rivers and adjacent seas, *Cont. Shelf. Res.*, 18, 859-882, 1998.

Guay, C. K. H., F. A. McLaughlin, and M. Yamamoto-Kawai, Differentiating fluvial components of upper Canada Basin waters on the basis of measurements of dissolved barium combined with other physical and chemical tracers, *J. Geophys. Res.*, 114, C00A09, doi:10.1029/2008JC005099, 2009.

Hansell, D.A., Kadko, D. and N. R. Bates, Degradation of terrigenous dissolved organic carbon in the western Arctic Ocean, *Science*, 304, 858–861, 2004.

Hoppema M., F. Dehairs, J. Navez, C. Monnin, C. Jeandel, E. Fahrbach, H. J. W. de Baar, Dissolved barium distributions in the Weddell Gyre: Impact of circulation and biogeochemical processes, *Marine Chemistry*, 122,118-129, 2010.

Horner, R., and G. C. Schrader, Relative Contributions of Ice Algae, Phytoplankton and Benthic microalgae to Primary Production in Nearshore Regions of the Beaufort Sea, *Arctic,* 35, 485-503, 1992.

Jacquet S. H. M., Barium in the Southern Ocean: Towards an estimation of twilight zone C mineralization. Doctoral Thesis. Vrije Universiteit Brussel, Belgium, 234 pp., 2007.

Jacquet, S. H. M., F. Dehairs, D. Cardinal, J. Navez, B.Dellile, Barium distribution across the Southern Ocean frontal system in the Crozel-Kerguelen Basin, *Mar. Chem.*, 95, 149-162, 2005.

Jacquet, S. H. M., F. Dehairs, M. Elskens, N. Savoye, and D. Cardinal, Barium cycling along WOCE SR3 line in the Southern Ocean, *Mar. Chem.*, 106, 33-45, 2007.

Juul-Pedersen, T., C. Michel, and M. Gosselin, Sinking export of particulate organic material from the euphotic zone in the eastern Beaufort Sea, *Mar. Ecol. Prog. Ser.*, 410, 55-70, 2010.

Kellogg, C. T. E., S. D. Carpenter, A. A. Renfro, A. Sallon, C. Michel, J. K. Cochran, and J. W. Deming, Evidence for microbial attenuation of particle flux in the Amundsen Gulf and Beaufort Sea: elevated hydrolytic enzyme activity on sinking aggregates, Pol. Biol., DOI 10.1007/s00300-011-1015-0, 2011.

Lanos, R., Circulation régionale, masses d'eau, cycles d'évolution et transports entre la mer de Beaufort et le golfe d'Amundsen. Ph.D. thesis, Université du Québec, 2009.

Lansard, B., A. Mucci, L. A. Miller, R. W. Macdonald, and Y. Gratton, Seasonal variability of water mass distribution in the southeastern Beaufort Sea determined by total alkalinity and $\delta^{18}O$, subm. to *J. Geophys. Res.*, 2011.

Lavoie, D., R. W. Macdonald, and K. L. Denman, Primary productivity and export fluxes on the

Canadian shelf of the Beaufort Sea: A modelling study, *J. Mar. Sys.*, 75, 17-32, 2009.

Macdonald, R. W., E. C. Carmack, F. McLaughlin, K. Iseki, D. Macdonald, and M. O'Brien, Composition and Modification of Water Masses in the Mackenzie Shelf Estuary, *J. Geophys. Res.*, 94(C12), 18057-18070, 1989.

Magen, C., G. Chaillou, S. A. Crowe, A. Mucci, B. Sundy, A. Gao, R. Makabe, and H. Sasaki, Origin and fate of particulate organic matter in the Southern Beaufort Sea – Amundsen Gulf region, Canadian Arctic, *Est. Coast. Shelf Science*, 86, 31-41, 2010.

Miller, L. A., T. N. Papakyriakou, R. E. Collins, J. W. Deming, J. K. Ehn, R. W. Macdonald, A. Mucci, O. Owens, M. Raudsepp, and N. Sutherland, Carbon dynamics in sea ice: A winter flux time series, *J. Geophys. Res.*, 116, C02028, doi:10.1029/2009JC006058, 2011.

Millero, F. J., Chemical Oceanography, 3rd ed., CRC press, Boca Raton, Fl, USA, 2006.

Monnin, C., A thermodynamic model for the solubility of barite and celestite in electrolyte solutions and seawater to 200 °C and 1 kbar, *Chem. Geol.*, 153(1-4), 187-209, 1999.

Monnin, C., C. Jeandel, T. Cattaldo, and F. Dehairs, The marine barite saturation state of the world's ocean, *Mar. Chem.*, 65, 253-261, 1999.

Mucci, A., B. Lansard, L. A.Miller, and T. N. Papakyriakou, CO_2 fluxes across the air-sea interface in the southeastern Beaufort Sea: the ice-free period, J. Geophys. Res. 115, C040003, doi:10.1029/2009JC005330, 2010.

Münchow, A. and H. Melling, Ocean current observations from Nares Strait to the west of Greenland: Interannual to tidal variability and forcing, *J. Mar. Res.*, 66, 801-833, 2008.

Mundy, C. J., M. Gosselin, J. Ehn, Y. Gratton, A. Rossnagel, D. G. Barber, J. Martin, J.-E. Tremblay, M. Palmer, K. R. Arrigo, G. Darnis, L. Fortier, B. Else, and T. Papakyriakou, Contribution of under-ice primary production to an ice-edge upwelling phytoplankton bloom in the Canadian Beaufort Sea, Geophys. Res. Lett., 36, L17601, doi:10.1029/2009GL038837, 2009.

Papakyriakou, T., and L. A. Miller, Springtime CO_2 exchange over seasonal sea ice in the Canadian Arctic Archipelago, *Annals of Glaciology*, 52(57), 215-224, 2011.

Prange, M., Einfluss arktischer Süsswasserquellen auf die Zirkulation im Nordmeer und im Nordatlantik in einem prognostischen Ozean-Meereis-Modell. Ph.D. thesis, University of Bremen, Bremen, Germany, 2002 (see also: http://www.whoi.edu/page.do?pid=30587).

Renaud, P. E., A. Riedel, C. Michel, N. Morata, M. Gosselin, T. Juul-Pedersen, and A. Chiuchiolo, Seasonal variation in benthic community oxygen demand: A respsonse to an ice algal bloom in the Beaufort Sea, Canadian Arctic?, *J. Mar. Sys.*, 67, 1-12, 2007.

Richerol, T., A. Rochon, S. Blasco, D. B. Scott, T. M. Schell, and R. J. Bennett, Distribution of dinoflagellate cysts in surface sediments of the Mackenzie Shelf and Amundsen Gulf, Beaufort Sea (Canada), *J. Mar. Sys.*, 74, 825-839, 2008.

Semiletov, I., A. Makshtas, S.-I. Akasofu, and E. Andreas, Atmospheric CO_2 balance: The role of Arctic sea ice, *Geophys. Res. Lett.*, 31, L05121, doi:10.1029/GL2003017996, 2004.

Shadwick, E. H., H. Thomas, Y. Gratton, D. Leong, S. Moore, T. N. Papakyriakou, and A. E. F. Prowe, Export of Pacific carbon through the Arctic Archipelago to the North Atlantic, *Cont. Shelf Res.,* 31, 806–816, doi:10.1016/j.csr.2011.01.014, 2011a.

Shadwick, E. H., H. Thomas, M. Chierici, B. Else, A. Fransson, C. Michel, L. A. Miller, A. Mucci, A. Niemi, T. N. Papakyriakou, and J.-É. Tremblay, Seasonal Variability of the Inorganic Carbon System in the Amundsen Gulf Region of the Southeastern Beaufort Sea, *Limnology and Oceanography*, 56, 303-322, 2011b

Sternberg, E., D. Tang, T.-Y. Ho, C. Jeandel, and F. M. M. Morel, Barium uptake and adsorption in diatoms, *Geochim. Cosmochim. Acta*, 69, 2745-2752, 2005.

Sternberg, E., C. Jeandel, J.-C. Miquel, B. Gasser, M. Souhaut, R. Arraes-Mescoff, and R. Francois, Particulate barium fluxes and export production in the northwestern Mediterranean, *Mar. Chem.*,

105, 281-295, 2007.

Sternberg, E., C. Jeandel, E. Robin, and M. Souhaut, Seasonal cycle of suspended barite in the mediterranean sea, *Geochim. Cosmochim. Acta*, 72, 4020-4034, 2008.

Taylor, J. R., K. K. Falkner, U. Schauer, and M. Meredith, Quantitative considerations of dissolved barium as a tracer in the Arctic Ocean, *J. Geophys. Res.*, 108(C12), 3374, doi:10.1029/2002JC001635, 2003.

Tremblay, J., K. Simpson, J. Martin, L. Miller, Y. Gratton, D. Barber, and N. M. Price, Vertical stability and the annual dynamics of nutrients and chlorophyll fluorescence in the coastal, southeast Beaufort Sea, *J. Geophys. Res.*, 113, C07S90, doi:10.1029/2007JC004547, 2008.

van Beek, P., E. Sternberg, J.-L. Reyss, M. Souhaut, E. Robin, and C. Jeandel, $^{228}Ra/^{226}Ra$ and $^{226}Ra/Ba$ ratios in the Western Mediterranean Sea: Barite formation and transport in the water column, *Geochimica et Cosmochimica Acta*, 73, 4720–4737, 2009.

Yamamoto-Kawai, M. and N. Tanaka, Freshwater and brine behaviors in the Arctic Ocean deduced from historical data of $\delta^{18}O$ and alkalinity (1992-2002 A.D.), *J. Geophys. Res.*, 110, C10003, 2005.

Yamamoto-Kawai, M., F. A. McLaughlin, E. C. Carmack, S. Nishino, and K. Shimada, Freshwater budget of the Canada basin, Arctic Ocean, from salinity, $\delta^{18}O$ and nutrients, *J. Geophys. Res.*, 113, C01007, 2008.

Yamamoto-Kawai, M., E. C. Carmack, F. A. McLaughlin, K. K. Falkner, Oxygen isotope ratio, barium and salinity in waters around the North American coast from the Pacific to the Atlantic: Implications for freshwater sources to the Arctic throughflow, *J. Mar Res.*, 68, 97–117, 2010.

Yi, Y., J. J. Gibson, J.-F. Hélie, and T. A. Dick, Synoptic and time-series stable isotope surveys of the Mackenzie River from Great Slave Lake to the Arctic Ocean, 2003 to 2006, *J. of Hydrology*, 383, 223-232, 2010.

Zemmelink, H. J., B. Delille, J. L. Tison, E. J. Hintsa, L. Houghton, and J. W. Dacey, CO_2 deposition over multi-year ice of the western Weddell Sea, *Geophys. Res. Lett.*, 33, doi:10.1029/2006GL026320, 2006.

Figure Captions

Figure 1: Investigation area. The stations sampled for dissolved Ba are indicated by red stars. The box encompasses the area 70°N-72°N, 121.8°W -126°W. The annual cycles and budgets reported in this paper were constructed from data collected at stations within this area. Hydrographic and carbonate system parameters are from higher temporal and spatial sampling densities [see *Shadwick et al.*, 2011b].

Figure 2: Temporal evolution of salinity in the surface waters of the Amundsen Gulf. Details of the seasonality of salinity and related carbon parameters have been discussed in detail by *Shadwick et al.* [2011b]. We have indicated the evolution of the S_P =33.1 isopleth, which represents the lower boundary of our analysis.

Figure 3: Dissolved Ba profiles from selected stations in the Canadian Arctic Archipelago and Baffin Bay. Individual dissolved Ba profiles are shown for four locations: the Mackenzie Shelf (purple line), the Amundsen Gulf (red line) and Lancaster Sound (green line), as well as near the west Greenland Coast (blue line). Please refer to insert for locations.

Figure 4: Distribution of dissolved Barium in the Canadian Arctic Archipelago. We show the distribution of dissolved Ba along 75°N from the eastern Beaufort Sea to Baffin Bay and a subsequent cross section through Nares Strait. Please note the different Ba characteristics on the eastern (west of approximately 70°W, [Ba]≈45 nM) and western (east of approximately 80°W, [Ba] ≈55 nM) sides of Nares Strait, respectively.

Figure 5: Distribution of Ba, $\delta^{18}O$, and A_T during Spring 2008. Dissolved Ba (a), $\delta^{18}O$ (b), and A_T

(c) in surface waters are shown as average observations made during the months of May, June and July 2008. The elevated Ba and lower A_T concentrations near the mouth of the Anderson River correspond to more negative $\delta^{18}O$ values [e.g., *Bates et al.*, 2009]. Following *Macdonald et al.* [1989] and *Bates et al.* [2009], freshwater from river runoff and sea-ice melt are distinguished on the basis of their salinity and $\delta^{18}O$ characteristics (d). The color coding in (d) indicates the longitude of the sampling location.

Figure 6: Relationship between carbonate system parameters and Ba. Ba vs. DIC (a, b) and Ba vs. A_T (c, d) are shown with corresponding depth (a, c) or salinity (b, d) values in color, respectively. The color coding does not reveal the full ranges of depth or salinity, but focuses on the 30-200 m depth range, where the gradients are strongest. Higher or lower values of salinity and depth are included within the maximum/minimum color, respectively. The lines are drawn to underline the conservative behaviour of Ba and A_T in the deeper waters, in contrast to DIC, which clearly reveals the addition of metabolic CO_2 as shown by *Shadwick et al.* [2011a, b]. The Pacific and deep Atlantic water masses are also called Upper and Lower Halocline Waters (UHL, LHL), respectively.

Figure 7: Temporal evolution of Ba, $\delta^{18}O$ and the barite saturation state in the Amundsen Gulf. Panel (a) shows the dissolved Ba concentrations for the water column of the Amundsen Gulf. In (b) and (c) we show $\delta^{18}O$ and the barite saturation state. We indicate the S_P = 33.1 isopleth, as well as the S_P = 32 isoline in (c), both encompassing approximately the depth range of 50 m to 100 m.

Figure 8: Property / property plots of Ba related and hydrographic parameters observed in the

Amundsen Gulf. For the entire water column in the Amundsen Gulf, the relationships of dissolved Ba (a) and the saturation state of barite (b) vs. salinity and vs. $\delta^{18}O$ (c, d) are shown, respectively. In (e) and (f) excerpts are shown for the upper part of the water column, i.e., for all samples with $S_P \leqq 33.1$ (see Fig. 2). Observed dissolved Ba concentrations (Ba_{obs}) are shown (blue dots), as well as the ideal Ba concentrations according to the three end-member mixing model (green diamonds). Furthermore, the model was run without riverine Ba ($Ba_{ideal}\{no\ Ba_{river}\}$, magenta triangles), which represents a conservative mixing between surface waters and UHL. The difference between Ba_{obs} and Ba_{ideal} (Ba deficiency) is attributed to Ba export (Ba_{exp}) via sinking of organic matter (i.e., as bio-Ba). The conservative behaviour of $Ba_{ideal}\{no\ Ba_{river}\}$ clearly emphasizes the importance of riverine Ba contributions to the surface layer Ba concentrations. Samples deeper than 50 m are plotted as open symbols, while shallower samples are plotted as filled symbols (e). For samples with $S_P \leqq 33.1$ we compare the observed barite saturation state (open symbols) with the barite saturation state computed with $Ba_{ideal}\{no\ Ba_{river}\}$. The Ba surplus at $S_P > 32$ is attributed to the decay of bio-Ba (f). Please note that no river contribution can be detected below 50 m, approximately corresponding to $S_P > 32$ (see also Fig. 7c). The dotted lines in all panels indicate the properties of the UHL waters (Table 1), and/or the equilibrium level of the barite saturation = 0.9-1.1, which inherently assumes an uncertainty of 10% in the computation of the barite saturation state [*Monnin et al.*, 1999].

Figure 9: Time series of Ba_{ideal}, Ba_{obs}, Ba_{export}, decay of bio-Ba, and NH_4^+ for Amundsen Gulf. The seasonality of Ba_{ideal} (a), Ba_{obs} (b) and Ba_{exp} (c) for the upper 50 m of the water column in Amundsen Gulf is shown for a full annual cycle. Please note the change in the color scale in (c). We computed the decay of bio-Ba in the subsurface layer of the Amundsen Gulf as difference from the observations and the assumed conservative mixing between the surface layer and the UHL (lower panel, see also Fig. 8f). The upper panel shows the integration of this Ba surplus over the depth range of 50 m to 100 m,

i.e., approximately over the S_P range 32 – 33.1. For comparison, we show the seasonal evolution of NH_4^+ in the upper water column of Amundsen Gulf. NH_4^+ can be considered as a tracer of respiratory activity, thus indicating the arrival of sinking particulate organic matter and the onset of its respiration in the subsurface layer [see also *Forest et al.*, 2011].

Figure 10: Temporal evolution of Ba-related inventories in the upper 50 m of the water column. Panel (a) shows the fraction of riverine Ba, which is exported. Panel (b) shows the temporal evolution of river runoff and NCP (NCP after *Shadwick et al.* [2011b] and river runoff after *Prange* [2002]; see also: Water survey of Canada, http://www.wsc.ec.gc.ca/staflo/index_e.cfm?cname=flow_daily.cfm). Export of Ba and derived carbon export are shown (c) as well as the fraction of Ba_{ideal}, which is exported. Squares indicate individual data, whereas shaded areas represent the monthly averages (a, c). The lowest fraction of riverine Ba (a) coincided with the salinity maximum, and the highest fraction with the salinity minimum, respectively. Increased Ba export (c) coincided with the under-ice algal bloom, slightly earlier than the arrival of riverine freshwater (b). Ba export exceeded the riverine Ba inputs. Ba and carbon exports peak in late summer, at the end of the biologically active period (b).

Figure 11: Carbon budget for Amundsen Gulf. Literature values and results of this work are used to estimate the carbon budget for the Amundsen Gulf. Since data were compiled from different years, the budget is climatological rather than for a specific year. Details of the individual terms are given in the text. Sources and times of observations: [a]*Shadwick et al.* [2011b]: 2007-2008; [b]*Forest et al.* [2011]: 2008; [c]Shadwick et al. [2011a]: 2007; [d]*Lanos* [2009]: 2002-2004; [f]*Renaud et al.* [2007]: 2004; [h]*Forest et al.* [2008]: 2003-2004.

Table 1: End-members and characteristics used for the water mass decomposition analysis. All data were measured during our cruises. The meteoric water concentrations were measured in the Horton River Estuary during our program in spring 2008. $\delta^{18}O$ for sea-ice melt is adapted from *Bates et al.* [2009]. Salinity and A_T were used in the decomposition analysis, whereas Ba was used to compute the "ideal" Ba concentrations. Note that values quoted below may differ from those used in other studies [*Chierici et al.*, 2011, this issue] in the same area because of spatial and temporal variability. Furthermore, the null salinity and alkalinity ascribed to the sea-ice melt water reflect the integrated annual effect of the ice cycle.

	A_T [µmol kg^{-1}]	Salinity (S_P)	Ba [nM]	$\delta^{18}O$ [‰]
Meteoric water	1880.0	0	295	-20
Sea-ice melt	0	0	0	-2.0
Upper Halocline water	2283.0	33.1	69	-1.5

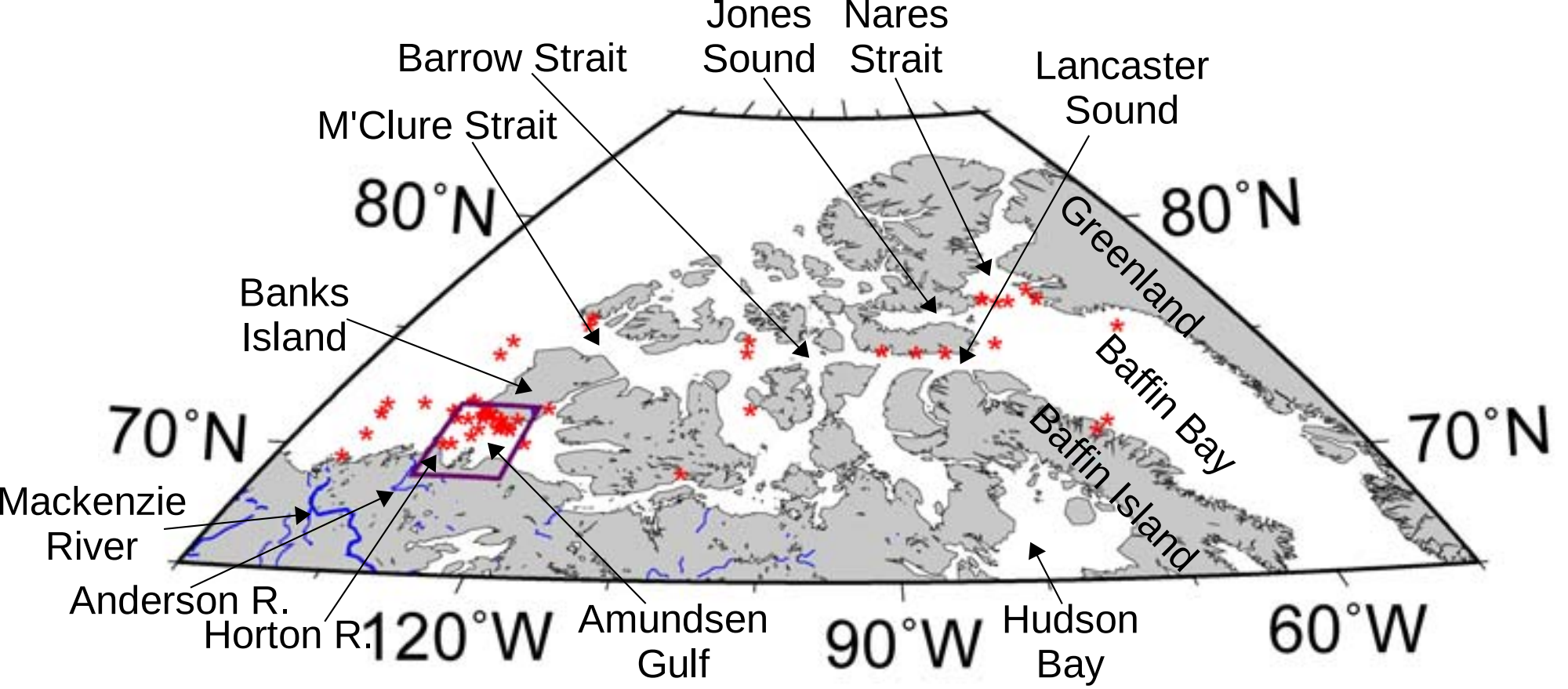
Barrow Strait
Jones Sound
Nares Strait
Lancaster Sound
M'Clure Strait
80°N
80°N
Greenland
Banks Island
Baffin Bay
70°N
70°N
Baffin Island
Mackenzie River
Anderson R.
Horton R.
120°W
Amundsen Gulf
90°W
Hudson Bay
60°W

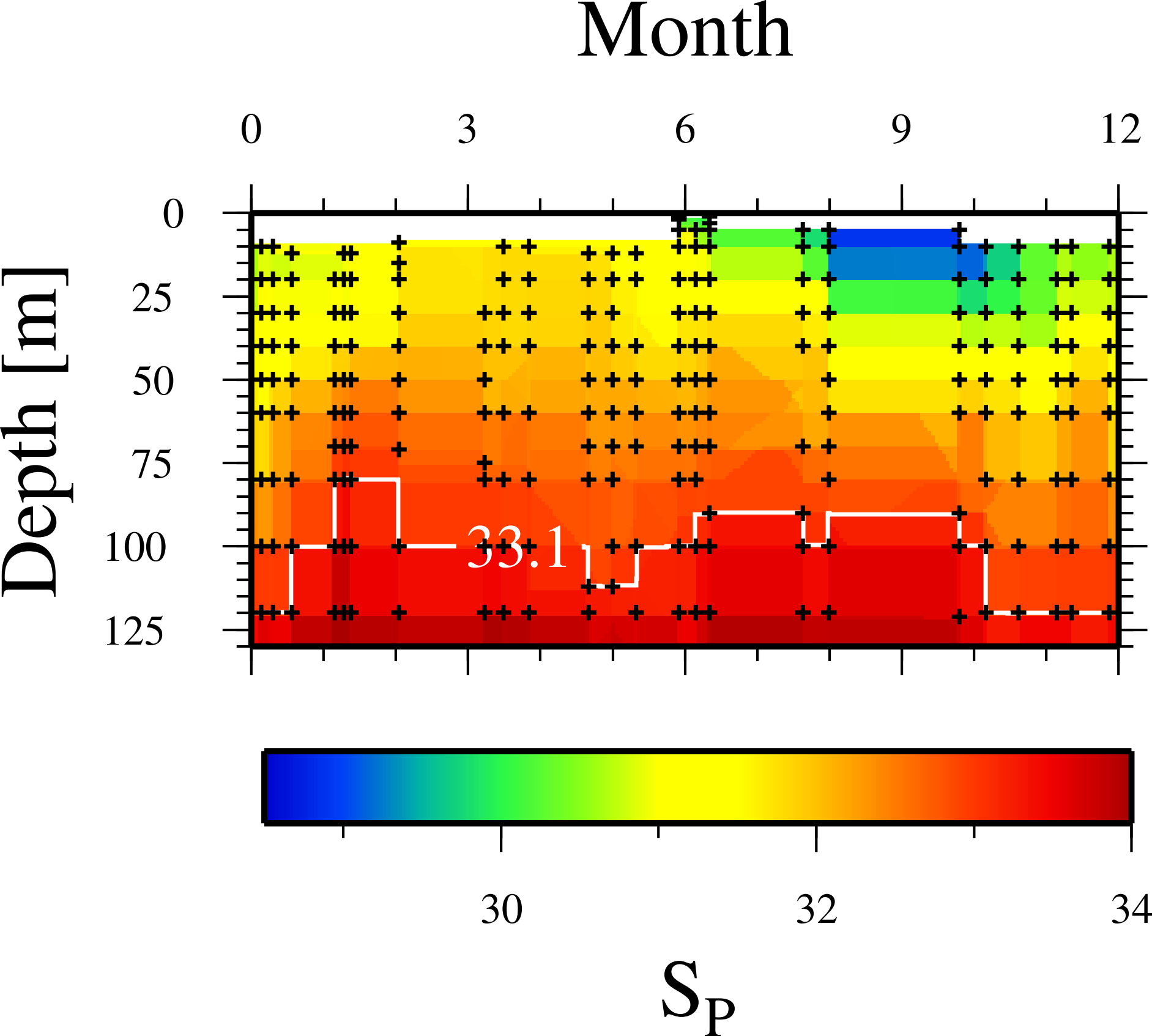
Month
0
3
6
9
12
Depth [m]
0
25
50
75
100
125
33.1
30
32
34
S_P

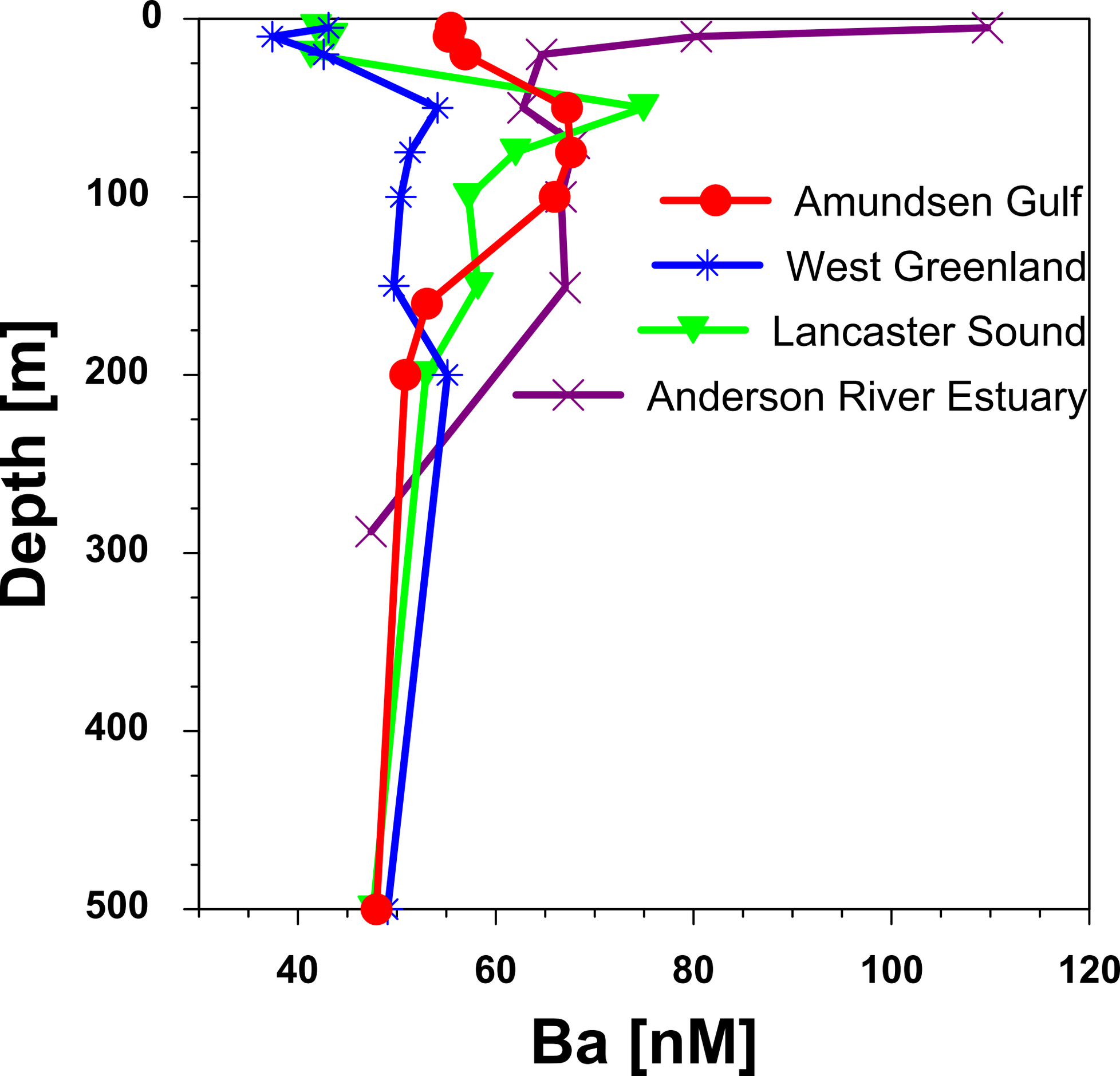
Depth [m]
0
100
200
300
400
500
40
60
80
100
120
Ba [nM]
Amundsen Gulf
West Greenland
Lancaster Sound
Anderson River Estuary

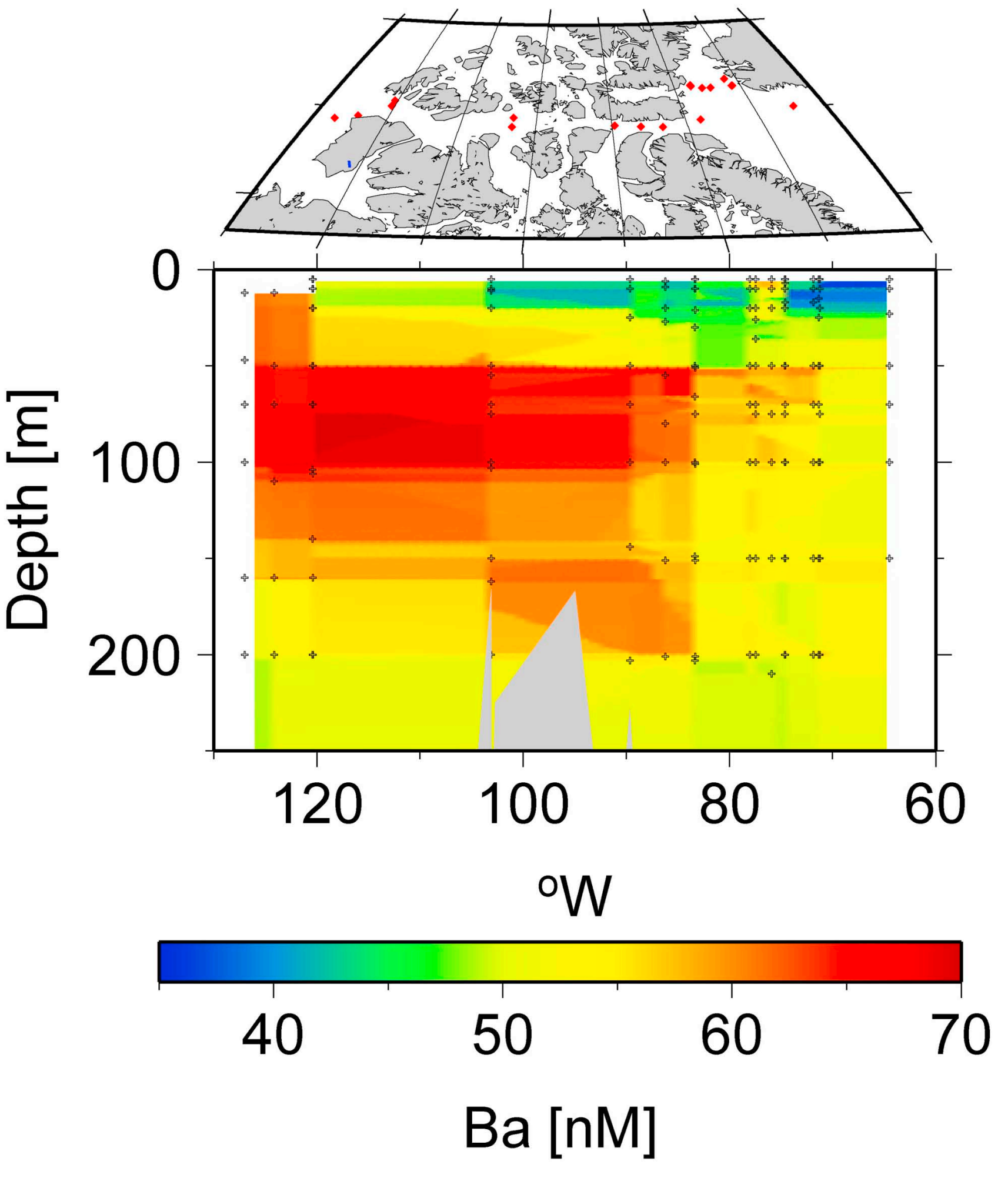
0
100
200
Depth [m]
120
100
80
60
°W
40
50
60
70
Ba [nM]

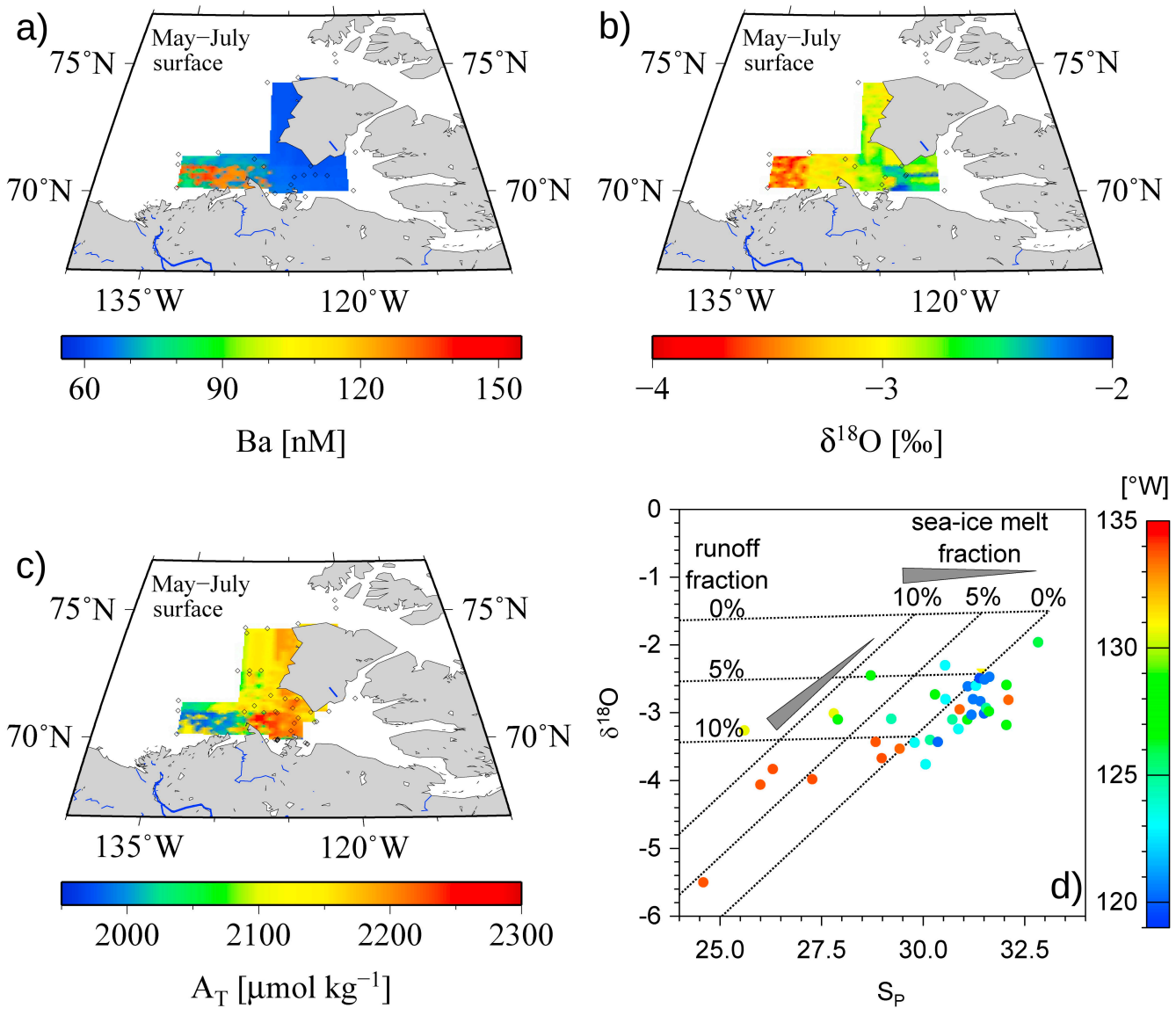
a)
May–July surface
75°N
70°N
135°W
120°W
60
90
120
150
Ba [nM]
b)
May–July surface
75°N
70°N
135°W
120°W
−4
−3
−2
δ18O [‰]
c)
May–July surface
75°N
70°N
135°W
120°W
2000
2100
2200
2300
AT [µmol kg−1]
d)
runoff fraction
0%
5%
10%
sea-ice melt fraction
10%
5%
0%
δ18O
SP
[°W]
135
130
125
120

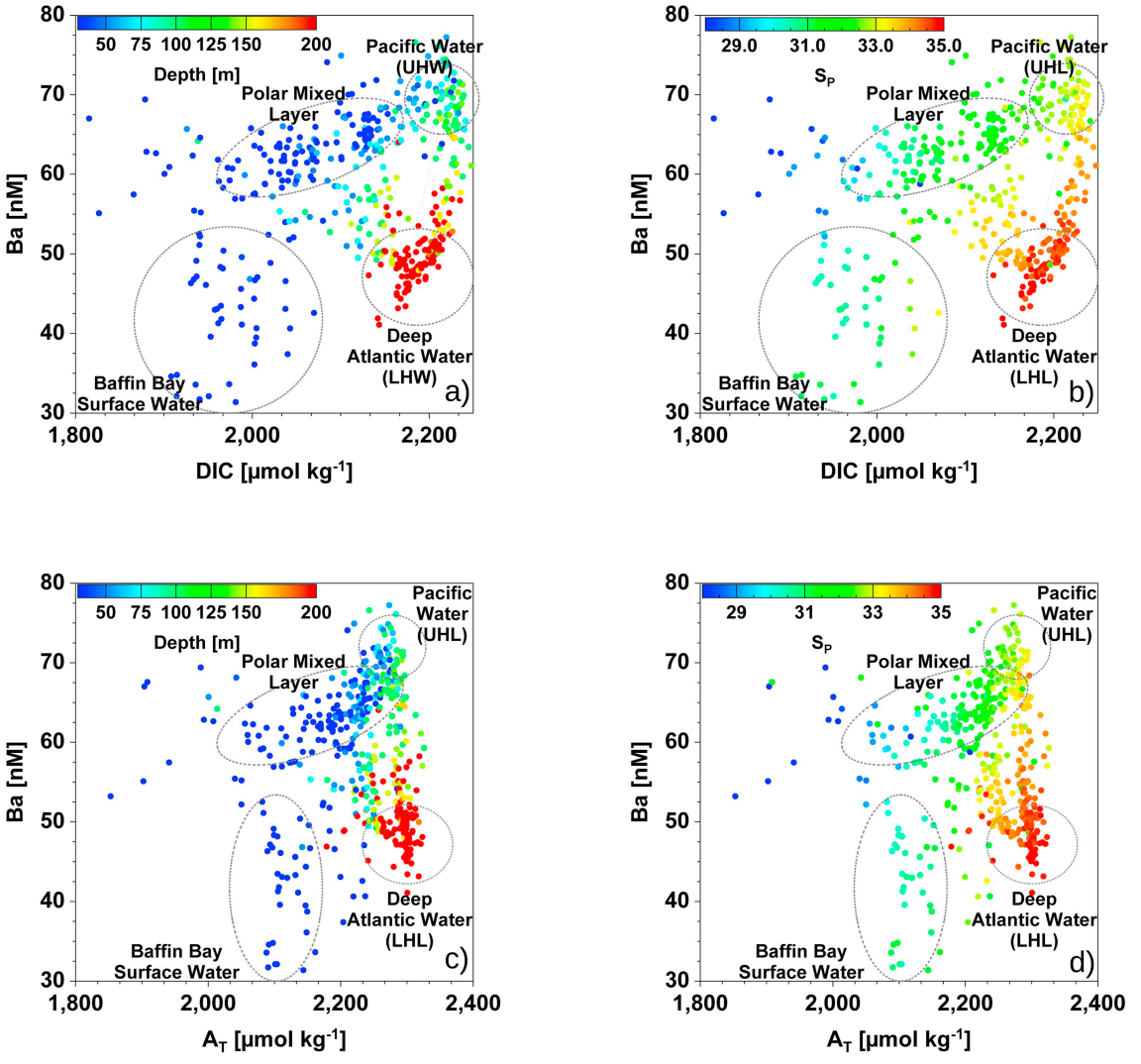
50 75 100 125 150 200
Depth [m]
Pacific Water (UHW)
Polar Mixed Layer
Deep Atlantic Water (LHW)
Baffin Bay Surface Water
a)
Ba [nM]
DIC [µmol kg-1]
29.0 31.0 33.0 35.0
SP
Pacific Water (UHL)
Polar Mixed Layer
Deep Atlantic Water (LHL)
Baffin Bay Surface Water
b)
50 75 100 125 150 200
Depth [m]
Pacific Water (UHL)
Polar Mixed Layer
Deep Atlantic Water (LHL)
Baffin Bay Surface Water
c)
AT [µmol kg-1]
29 31 33 35
SP
Pacific Water (UHL)
Polar Mixed Layer
Deep Atlantic Water (LHL)
Baffin Bay Surface Water
d)

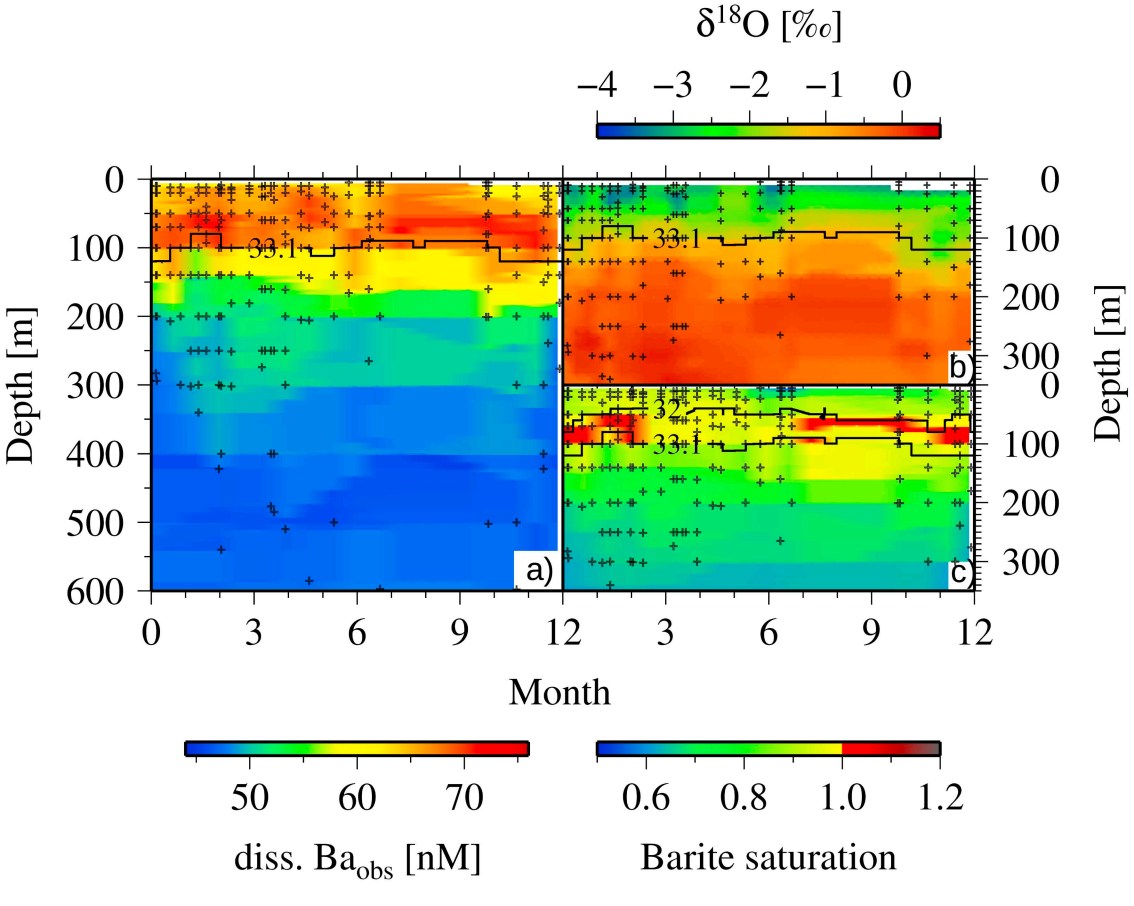
δ18O [‰]
−4 −3 −2 −1 0
Depth [m]
0 100 200 300 400 500 600
33.1
a)
b)
c)
32
33.1
0 3 6 9 12 3 6 9 12
Month
50 60 70
diss. Baobs [nM]
0.6 0.8 1.0 1.2
Barite saturation

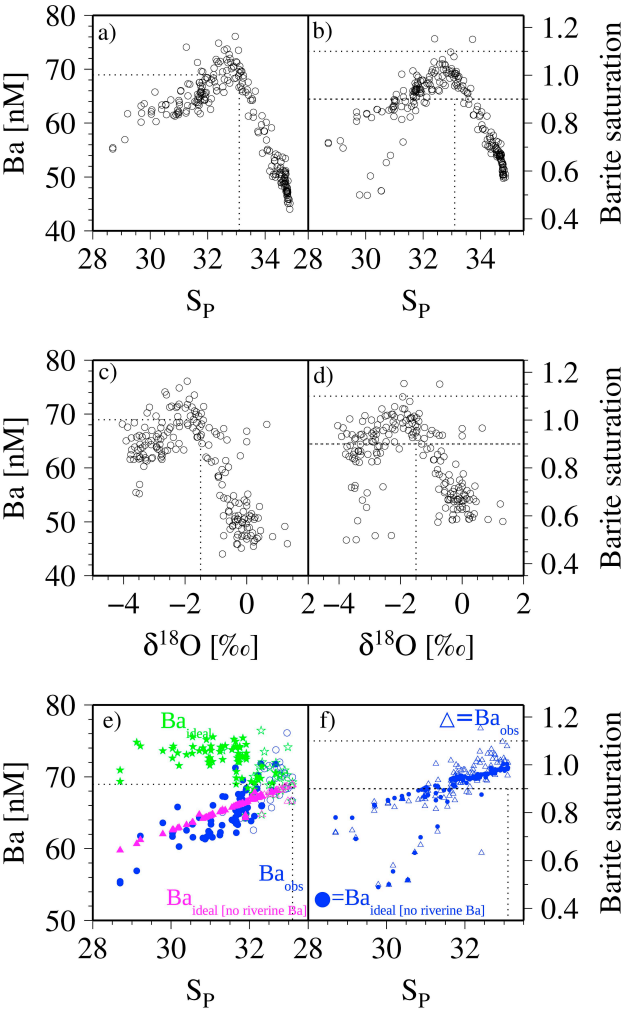
a)
b)
c)
d)
e)
f)
Ba [nM]
Barite saturation
S_P
δ18O [‰]
Ba ideal
Ba obs
Ba ideal [no riverine Ba]
△=Ba obs
●=Ba ideal [no riverine Ba]

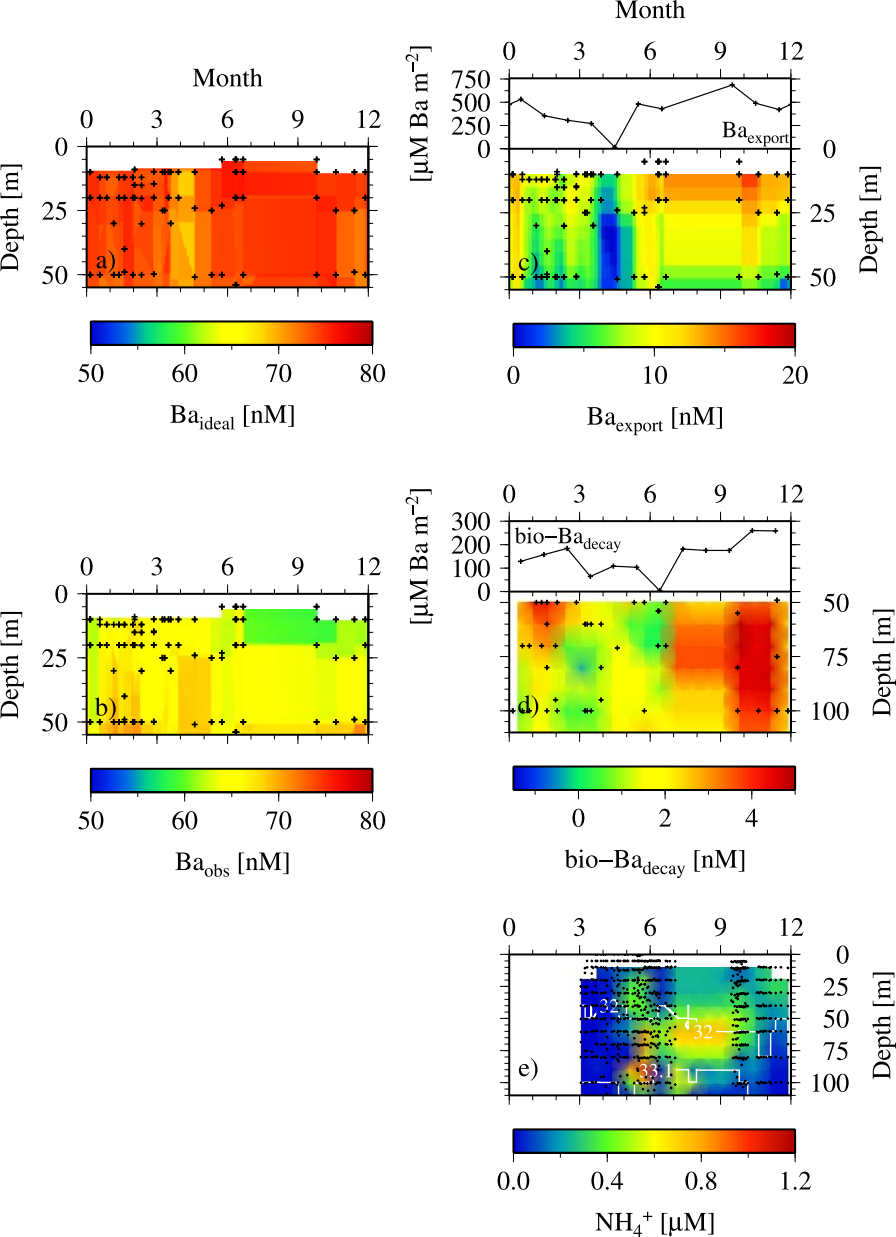
Month
0 3 6 9 12
Depth [m]
0
25
50
a)
50 60 70 80
Ba$_{ideal}$ [nM]
[µM Ba m^{-2}]
750
500
250
0
Ba$_{export}$
c)
0 10 20
Ba$_{export}$ [nM]
b)
Ba$_{obs}$ [nM]
bio−Ba$_{decay}$
300
200
100
d)
bio−Ba$_{decay}$ [nM]
e)
32
33.1
0.0 0.4 0.8 1.2
NH$_4^+$ [µM]

Month
0
3
6
9
12
a)
b)
c)
20
15
10
5
0
$Ba_{riverine}$ of Ba_{ideal} [%]
30000
20000
10000
◆ Runoff
[m^3 s^{-1}]
1.0
0.5
0.0
−0.5
☆ NCP
[mol C m^{-2} $month^{-1}$]
600
400
200
0
Ba export
[µM Ba m^{-2}]
Ba_{export} of Ba_{ideal} [%]
1.5
1.0
0.5
0.0
C export
[mol C m^{-2}]
Month

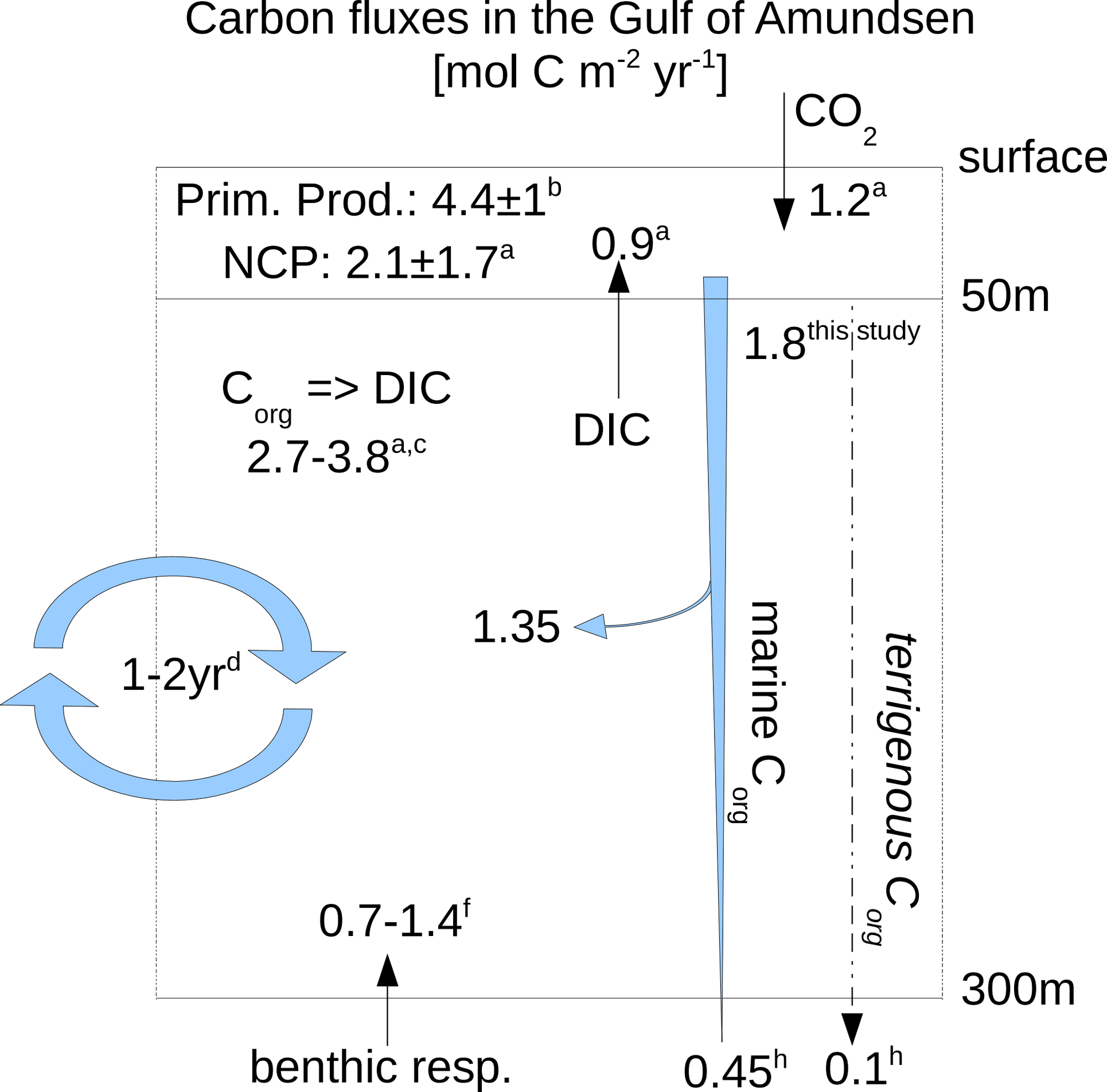
Carbon fluxes in the Gulf of Amundsen
[mol C m-2 yr-1]
CO2
surface
Prim. Prod.: 4.4±1b
NCP: 2.1±1.7a
1.2a
0.9a
50m
1.8this study
Corg => DIC
2.7-3.8a,c
DIC
1.35
1-2yrd
marine Corg
terrigenous Corg
0.7-1.4f
300m
benthic resp.
0.45h
0.1h